Geochemistry Geophysics Geosystems G3
AN ELECTRONIC JOURNAL OF THE EARTH SCIENCES
Published by AGU and the Geochemical Society

Article
Volume 10, Number 6
24 June 2009
Q06015, doi:10.1029/2009GC002386
ISSN: 1525-2027

Intraplate volcanism with complex age-distance patterns: A case for small-scale sublithospheric convection

M. D. Ballmer
Institute of Geophysics, ETH Zurich, CH-8092 Zurich, Switzerland (ballmer@tomo.ig.erdw.ethz.ch)

J. van Hunen
Department of Earth Sciences, Durham University, Durham DH1 3LE, UK

G. Ito and T. A. Bianco
SOEST, University of Hawai'i at Mānoa, Honolulu, Hawaii 96822, USA

P. J. Tackley
Institute of Geophysics, ETH Zurich, CH-8092 Zurich, Switzerland

[1] Many volcano chains in the Pacific do not follow the most fundamental predictions of hot spot theory in terms of geographic age progressions. One possible explanation for non–hot spot intraplate volcanism is small-scale sublithospheric convection (SSC), and we explore this concept using 3-D numerical models that simulate melting with rheology laws that account for the effects of dehydration. SSC spontaneously self-organizes beneath relatively mature oceanic lithosphere. Whenever this lithosphere is sufficiently young and thin, SSC replaces the shallow layer of harzburgite, which was formed by partial melting at the mid-ocean ridge, with fresh peridotite. This mechanism enables magma generation without any preexisting thermochemical anomalies. However, the additional effect of melting-induced dehydration to stiffen the harzburgite requires lower background viscosities to allow for vigorous SSC, overturn of the compositional stratification, and related magmatism. The intrinsic stiffness of the dehydrated harzburgite furthermore restricts penetration of SSC into very shallow and cooler levels. On the one hand, such a restriction precludes high degrees of melting, but on the other hand, it slows asthenospheric cooling and thus prolongs the duration of melting (to ~25 Ma). Volcanism over such an elongated melting anomaly continues for at least 10–20 Ma and occurs on seafloor ages of ~20 to ~60 Ma. These seafloor ages increase with increasing mantle temperature due to the effect of forming a thicker harzburgite layer from more extensive mid-ocean ridge melting. The long durations of volcanism predicted reconcile observations of extended activity of individual seamounts and synchronous activity over great distances along some volcanic chains. SSC thus gives an explanation for previously enigmatic volcano ages along the Line Islands and the Gilbert and Pukapuka ridges, as well as along the individual subchains of the Wakes, Marshalls, and Cook-Australs.

Components: 13,622 words, 11 figures, 2 tables.

Keywords: mantle convection; intraplate volcanism; Pukapuka; Cook-Austral Islands; Marshall Islands; numerical modeling.

Index Terms: 8415 Volcanology: Intra-plate processes (1033, 3615); 8011 Structural Geology: Kinematics of crustal and mantle deformation; 3225 Mathematical Geophysics: Numerical approximations and analysis (4260).

Received 15 January 2009; **Revised** 15 April 2009; **Accepted** 5 May 2009; **Published** 24 June 2009.

Ballmer, M. D., J. van Hunen, G. Ito, T. A. Bianco, and P. J. Tackley (2009), Intraplate volcanism with complex age-distance patterns: A case for small-scale sublithospheric convection, *Geochem. Geophys. Geosyst.*, *10*, Q06015, doi:10.1029/2009GC002386.

1. Introduction

[2] Oceanic intraplate volcanism has mostly been attributed to hot spots as caused by deep rooted mantle plumes [*Morgan*, 1971, 1972]. This theory has successfully predicted the behavior seen in many volcano chains of alignment with absolute plate motion and of a linear age-distance relationship, two features that are expected to be robustly developed on the fast Pacific Plate. Many volcano chains, however, do not display linear age-distance relationships including the Marshalls, Cook-Australs, Line Islands, Pukapuka, Gilbert ridges, and Wake seamounts [*Koppers et al.*, 2003, 2007; *McNutt et al.*, 1997; *Bonneville et al.*, 2006; *Davis et al.*, 2002; *Sandwell et al.*, 1995], which therefore call for an alternative mechanism.

[3] A mechanism that has often been invoked to account for non–hot spot intraplate volcanism is lithospheric cracking. Cracks parallel to plate motion may be induced by distal tensile stresses, or by thermal contraction [*Gans et al.*, 2003; *Sandwell and Fialko*, 2004; *Foulger*, 2007]. However, the cracking hypothesis does not provide an explanation for magma generation [e.g., *Lynch*, 1999]; it rather presumes a broad reservoir of preexisting partial melt in the asthenosphere to be tapped [*Anderson and Bass*, 1984; *Anderson*, 2000]. Such a layer of partial melt was originally proposed to account for low shear wave velocities in the asthenosphere [*Anderson and Sammis*, 1970]. However, since stiffening due to dehydration of olivine during melting probably dominates melt lubrication [*Karato*, 1986], such a reservoir is at odds with vertical viscosity profiles derived from postglacial rebound or geoid inversions [e.g., *Cadek and Fleitout*, 2003]. Moreover, alternative explanations for low velocities of seismic shear waves have been established [*Karato and Jung*, 1998; *Faul and Jackson*, 2005; *Stixrude and Lithgow-Bertelloni*, 2005; *Priestley and McKenzie*, 2006]. While the surface morphology of intraplate volcanoes may be influenced by tensional cracks [*Lynch*, 1999], it is unlikely that they control timing and location of volcanism.

[4] Gravity and seismic observations around the Pukapuka and neighboring ridges provide independent evidence that other mechanisms than lithospheric cracking generate these volcanic ridges c. These mechanisms include (1) channelized return flow of hot and fertile parcels of mantle toward the mid-ocean ridge (MOR) [*Weeraratne et al.*, 2007; *Sleep*, 2008] and (2) small-scale sublithospheric convection (SSC) [*Haxby and Weissel*, 1986; *Buck and Parmentier*, 1986; *Marquart*, 2001]. Whereas channelized return flow predicts slow and relatively steady age progressive volcanism toward younger seafloor ages, SSC may account for more complex age-distance patterns with quasi-synchronous volcanism over great distances [*Bonatti and Harrison*, 1976; *Bonatti et al.*, 1977; *Ballmer et al.*, 2007]. The Marshalls, Gilberts, Cook-Australs and the Wake seamounts display such highly complex age-distance patterns with intermittent activity at individual seamounts and synchronous activity over distances up to ~1500 km [*Duncan and McDougall*, 1976; *Turner and Jarrard*, 1982; *Chauvel et al.*, 1997; *Koppers et al.*, 2003]. Along Pukapuka, one may instead interpret sample ages as a systematic progression [*Sandwell et al.*, 1995], which would, however, be too fast to be reconciled with a hot spot or channelized return flow [cf. *Sleep*, 2008]. Along these lines, we suppose that SSC is a more likely mechanism for non–hot spot intraplate volcanism.

[5] SSC is predicted to spontaneously occur beneath mature oceanic seafloor owing to instabilities near the base of the lithospheric thermal boundary layer, at which the age of the seafloor at the onset of SSC depends on asthenospheric viscosity [*Richter*, 1973; *Richter and Parsons*, 1975]. After its onset, it organizes as rolls aligned by plate motion with a typical spacing of 200–250 km [*van Hunen et al.*, 2003; *Korenaga and Jordan*, 2004]. Thereafter, SSC removes the bottom of the depleted harzburgite layer (DHL), the residual from melting at the MOR, and replaces it by warm and fertile peridotite from below [*Ballmer et al.*, 2007]. Accordingly, SSC upwellings potentially spawn decompression melting (Figure 1) by over-

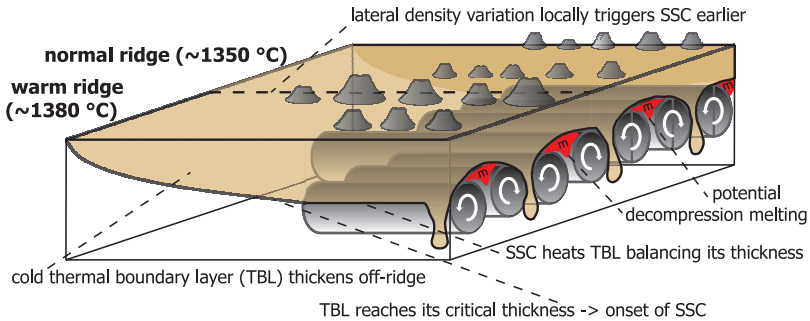

Figure 1. Small-scale sublithospheric convection (SSC) spontaneously evolves at the bottom of mature oceanic lithosphere. The age of the lithosphere, beneath which SSC first develops, varies with T_m, η_{eff}, and the extent of lateral density heterogeneity. SSC organizes as rolls aligned by plate motion with the possibility of decompression melting above its upwellings.

turning the thermal and compositional stratification at the base of the oceanic lithosphere.

[6] The intrinsic stiffness of the DHL [*Hirth and Kohlstedt*, 1996] may, however, complicate its removal [*Lee et al.*, 2005; *Afonso et al.*, 2008] by SSC and subsequent melting. Partial melting affects mantle density because of both melt retention and depletion [*Tackley and Stevenson*, 1993; *Schmeling*, 2000], and viscosity because of both dehydration and melt lubrication [*Hirth and Kohlstedt*, 2003], effects that have a strong feedback on convective flow. Dehydration during MOR melting produces a stiff DHL making the base of the lithosphere effectively equivalent to that of the DHL [*Hirth and Kohlstedt*, 1996] (rather than to the depth of an isotherm). Whereas the basic effects of stable density layering and of the feedback between melting and density variations on SSC have been investigated in 2-D [*Tackley and Stevenson*, 1993; *Schmeling*, 2000; *Raddick et al.*, 2002; *Zaranek and Parmentier*, 2004; *Hernlund et al.*, 2008], the 3-D behavior and effects of a compositionally dependent rheology (CRh) on SSC melting remain to be systematically explored.

[7] We aim to explore the effect of CRh on onset ages and geometries of SSC and associated melting through 3-D numerical modeling. We commence with presenting the predictions of two reference models. Subsequently, we compare onset ages and flow geometries of SSC for models with and without CRh. We continue exploring the systematics of onset ages, as well as of the durations and amounts of melting (and those of volcanism) for a broad set of parameters placing models with CRh over against models without CRh. Such a detailed study finally serves to explore whether SSC is a realistic mechanism to explain volcano chains with complex age-distance patterns also in the presence of a stiff DHL.

2. Methods

[8] Prior studies of viscous mantle flow with variable compositional buoyancy and rheology that are modified by partial melting were mostly applied only in 2-D. To explore thermochemical convection in 3-D we use an extended version of the finite element code CITCOM [*Moresi and Gurnis*, 1996; *Zhong et al.*, 2000]. The method described here for cases without CRh is equivalent to that used by *Ballmer et al.* [2007].

[9] In our models, properties that are passively advected on tracers (i.e., melt fraction φ and depletion of the residue F) are strongly time-dependent because of partial melting and refreezing. As F and φ crucially determine mantle density and viscosity η with a feedback on magma generation itself, a semi-implicit time integration scheme is required. We find that the numerical solution of problems including such feedback mechanisms otherwise depends on the lengths of time steps (for both CRh and no-CRh). Therefore, we extended CITCOM to include a predictor-corrector scheme [e.g., *van Keken*, 1993].

[10] We solve the nondimensional equations for conservation of mass, momentum, and energy for an incompressible, infinite Prandtl number fluid. We apply the extended Boussinesq approximation in order to include the effects of latent heat of

Table 1. Parameters, Parameter Variations, and Default Values[a]

Parameter	Variation	Unit
η_{eff} (at ξ = 1)	1.2×10^{19} to 5×10^{19}	Pa s
η_{eff} (at ξ = 10)	3.6×10^{18} to 5.4×10^{18}	Pa s
η_{eff} (at ξ = 40)	1.5×10^{18} to 4.2×10^{18}	Pa s
η_{eff} (at ξ = 100)	1.2×10^{18} to 1.6×10^{18}	Pa s
T_m	1350–1410 (1380)	°C
c_O	75–200 (125)	wt ppm
φ_C	0.1–2.0 (1.0)	%
ξ	1–100 (1, 40)	
ζ	0, 40	
v_{eff}	2–70 (55)	km/Ma
$\Delta\rho_F$	−300–0 (−72.6)	kg/m^3
$\Delta\rho_\varphi$	−500	kg/m^3
ρ_0	3300	kg/m^3
T_s	0	°C
E^*	1.2×10^5	J/mol
V^*	5×10^{-6}	m^3/mol
α	3×10^{-5}	K^{-1}
c_P	1250	J/kg/K
κ	1×10^{-6}	m^2/s
L	6.5×10^5	J/kg
γ	0.3	K/km

[a] Default values are given in parentheses. For explanation of symbols see Table 2.

melting, adiabatic heating, and viscous dissipation [*Christensen and Yuen*, 1985]:

$$\nabla \cdot u = 0, \tag{1}$$

$$\nabla\left[\eta\left(\nabla u + \nabla^T u\right)\right] - \nabla \cdot P = -RaT \cdot \hat{z} - RbF \cdot \hat{z} - Rc\varphi \cdot \hat{z}, \tag{2}$$

$$\frac{\partial T}{\partial t} + u \cdot \nabla T = \nabla^2 T + L\left(\frac{\partial F}{\partial t} + u \cdot \nabla F\right) + \frac{Di}{Ra}\eta\dot{\varepsilon}^2 + yu_z, \tag{3}$$

with $\boldsymbol{u}$, T, $\hat{z}$, P, t, ε, L and γ the velocity vector, temperature, vertical unit vector, dynamic pressure, time, strain, latent heat of melting and adiabatic gradient, respectively (Table 1).

[11] The governing dimensionless parameters *Ra*, *Di*, *Rb* and *Rc* are the thermal Rayleigh number, dissipation number, depletion Rayleigh number and melt retention Rayleigh number, respectively:

$$Ra = \frac{\alpha(T_m - T_s)\rho_0 g h^3}{\kappa\eta_0}, \tag{4}$$

$$Di = \frac{\alpha g h}{c_P}, \tag{5}$$

$$Rb = \frac{\Delta\rho_F g h^3}{\kappa\eta_0}, \tag{6}$$

$$Rc = \frac{\Delta\rho_\varphi g h^3}{\kappa\eta_0}, \tag{7}$$

with α, T_m, T_s, g, h, c_P, κ, η_0, ρ_0, $\Delta\rho_F$ and $\Delta\rho_\varphi$, the thermal expansivity, reference temperature, surface temperature, gravity acceleration, model scale height, specific heat, thermal diffusivity, reference viscosity, reference density, density anomaly related to 100% depletion, and density anomaly related to 100% melt retention, respectively. We define the effective viscosity: $\eta_{eff} = 0.0353\eta_0$ in cases with CRh, and $\eta_{eff} = 0.0311\eta_0$ in cases without. η_{eff} is tuned to represent the minimum viscosity in a vertical profile (i.e., in the asthenosphere) just before the onset of SSC. Hereinafter, η_{eff} is used to represent the dynamical behavior of our models (instead of Ra or η_0), because it is a more intuitively understandable variable.

[12] We model hydrous peridotite melting according to *Katz et al.* [2003] as valid in the shallow upper mantle. They relate the degree of batch melting to lithostatic pressure p, temperature T, and to water concentration in the solid c with an empirically fitted solidus. Water strongly reduces solidus temperatures at incipient melting, where depletion F is smallest. Even for rather low bulk water concentrations c_O of 0.0075–0.02 wt % as predicted for the upper mantle [*Hirth and Kohlstedt*, 1996], the solidus reduction is significant (i.e., 35 K up to 72 K). Retained melt refreezes to the extent given by the melting function as soon as temperatures decrease (i.e., $\partial T/\partial t + u \cdot \nabla T < 0$) or lithostatic pressure increases, and F and φ are reduced accordingly.

[13] We parameterize melt migration and extraction by using the dynamic melting approximation [*McKenzie*, 1985]. Magma is accumulated until a critical porosity φ_C is reached, at which point melt in an interconnected network becomes mobile [*Faul*, 2001]. Any excess melt fraction is instantaneously removed to maintain this porosity assuming that the time scales of melt extraction and migration through the overlying column of the mantle are much smaller than that of mantle flow.

[14] Water behaves like an incompatible element and thus preferentially partitions into the melt. We apply a partitioning coefficient for water of D_{H2O} =

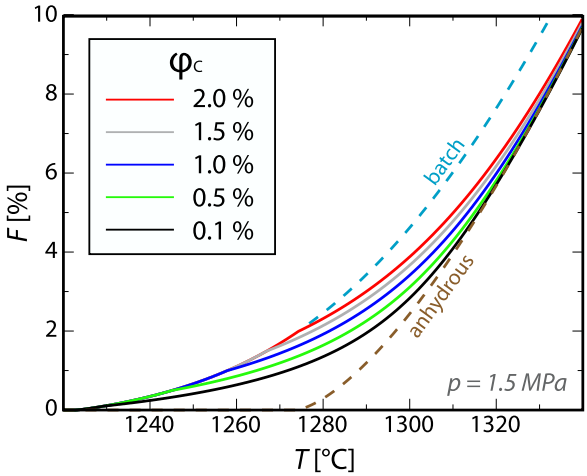

Figure 2. Dynamic melting curves (with $c_O = 125$ ppm) for various critical porosities φ_C are compared to batch melting (with c_O = 125 ppm) and anhydrous batch melting curves. The temperature required for a certain degree of melting (at intermediate degrees) is higher for small φ_C because of an earlier water separation from the solid.

0.01, similar to that for Ce [*Katz et al.*, 2003]. Before the initiation of melt extraction, water content in the solid c rapidly decreases with F:

$$c = D_{H2O}\frac{c_O}{F + D_{H2O}(1-F)} \tag{8}$$

With continuous melt extraction (at $\varphi = \varphi_C$) taking over, water starts to be efficiently removed from the system causing c to drop even more rapidly [*Zou*, 1998]:

$$c = D_{H2O}\frac{c_O\left(1-\frac{F-\varphi_c}{1-\varphi_c}\right)^{\frac{1}{\varphi_c+(1-\varphi_c)D_{H2O}}-1}}{F + D_{H2O}(1-F)} \tag{9}$$

Hence, c is a function of F, φ_C, and c_O ($c = c_O$ at $F = 0$).

[15] We self-consistently incorporate these effects of dehydration (i.e., equations (8) and (9)) into the melting law (Figure 2). This is equivalent to extending the melting relation of *Katz et al.* [2003] from batch melting to dynamic melting neglecting the effects of dynamic melting on major element partitioning. This simplification is valid for low degrees of melting (as maintained in this study), at which the effects of water on melting temperatures are greatest [*Katz et al.*, 2003].

[16] We use a Newtonian rheology dependent on temperature, depth, melt and water content:

$$\eta = \eta_0 \exp\left(\frac{E^* + \rho_0 g z V^*}{RT} - \frac{E^*}{RT_m} - \zeta_\varphi\right)\frac{(c_0 - c_{dry})\xi}{(c - c_{dry})\xi + c_0 - c}, \tag{10}$$

at which R, ξ, ζ, E^* and V^* are the ideal gas constant, dehydration stiffening coefficient, melt lubrication exponent, activation energy and activation volume, respectively. As shown from laboratory experiments for olivine, η is inversely correlated to c [*Karato et al.*, 1986; *Hirth and Kohlstedt*, 1996, 2003]. By definition, ξ is the viscosity contrast between a hydrated peridotite (with c = 125 ppm) and a depleted peridotite with dry olivine (with $c \leq c_{dry} \equiv 6$ wt ppm). The coefficient ξ is not fully constrained but may be enveloped by 10 and 100 [*Hirth and Kohlstedt*, 1996]. Furthermore, viscosity is exponentially related to melt content in such a manner that presence of significant melt fractions reduces the strength of peridotite. However, the stiffening effect of water exhaustion due to its incompatible behavior during melting dominates melt lubrication for realistic parameters (i.e., $\xi \geq 10$, $\zeta = 40$, $\varphi_C \leq 2\%$ [cf. *Karato*, 1986]). In a subset of our models, we neglect the effects of composition on rheology by setting ξ to one and ζ to zero. For all models, we apply a low value for E^* (120 kJ/mol) in order to mimic the contribution of dislocation creep in the asthenosphere with a simple Newtonian rheology [*Christensen*, 1984]. Higher values would underestimate lithospheric erosion induced by SSC [*van Hunen et al.*, 2005].

[17] Calculations are performed in a Cartesian box 3000 km long, 690–920 km wide and 400 km deep using from 384 × 96 × 48 up to 512 × 128 × 64 elements. We apply free-slip boundary conditions at the sides. Furthermore, we impose temperatures at the top and bottom of the model to be $T_{top} = 0$ and $T_{bot} = 1 + \gamma h$, respectively. As for the mechanical boundary conditions, the bottom and the top are imposed to move horizontally at v_{top} and at v_{bot} = 10 km/Ma, respectively. Imposing $v_{bot} > 0$ is done in order to simulate a realistic large-scale background flow. Thus, the effective plate velocity v_{eff} corresponds to the difference between v_{top}, and v_{bot} (v_{top} and v_{bot} are measured relative to the MOR).

[18] The inflow vertical side boundary corresponds to a plane parallel to the MOR and 260–1040 km

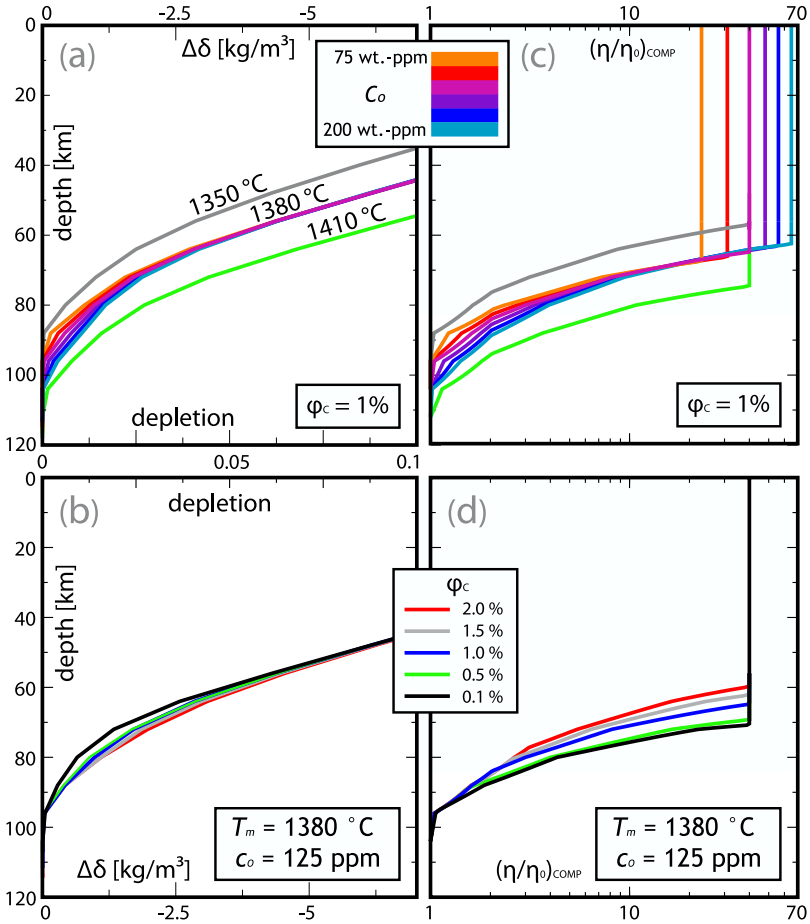

Figure 3. Vertical profiles of ridge melt depletion (a) for various T_m and c_O, as well as (b) for various φ_C obtained from 2-D simulations of flow and melting at the MOR are used to compute (c and d) vertical profiles of the compositional effect on rheology $(\eta/\eta_0)_{\mathrm{COMP}}$ valid for CRh (ξ = 40) and c_O = 125 ppm.

away from it. The MOR itself is not included, but the distal effects are simulated by imposing the appropriate inflow temperature and depletion profiles taken from 2-D models that include melting and lithosphere accretion at a MOR using the same physical parameters as the discussed 3-D calculations. The depletion profiles shown in Figures 3a and 3b are used to calculate the initial compositional rheological stratification for CRh. With depletion increasing upward, peridotite progressively dehydrates and hence stiffens (Figures 3c and 3d). Cases with higher mantle temperatures and water contents predict more extensive melting at the MOR and the formation of a thicker DHL, and hence a thicker effective lithosphere (Figures 3a and 3c). Simulations with higher water contents c_O than 125 ppm lead to a thicker base of the DHL, and further, to a DHL with a larger total viscosity contrast, because the initial mantle material is weaker compared to cases with the default c_O = 125 ppm. Cases with a larger critical porosity (φ_C) predict the DHL to be slightly more depleted at its base because of slower separation of water from the solid (Figure 3b) during MOR melting. As water separation crucially affects the vertical viscosity profile, the rigid lithosphere is thinnest for cases with large φ_C, although the harzburgite layer is thickest (Figure 3d).

3. Results

3.1. General Behavior of Reference Cases

3.1.1. Case A, Without Compositional Rheology

[19] In the reference case A (no-CRh, with default parameters (Table 1) at ξ = 1 and $\eta_{eff} = 1.6 \times 10^{19}$ Pa s) with purely p- and T-dependent rheology (i.e., without CRh), SSC (acronyms are listed in Table 2) spontaneously develops beneath a 26 Ma old lithosphere from the initial conditions that include

Table 2. Explanations for Abbreviations and Symbols as Used in Sections 3 and 4

Abbreviation	Definition
BDM	buoyant decompression melting
DHL	depleted harzburgite layer
CRh	compositional rheology
MOR	mid-ocean ridge
SSC	small-scale convection
SPSS	South Pacific Superswell
TBL	thermal boundary layer
d_{TBL}	convectible TBL thickness
d_{crit}	critical TBL thickness
M	melt volume produced per km of plate
T_m	reference mantle temperature
v_{eff}	absolute plate motion
c_O	bulk water content
$\Delta\rho_F$	density anomaly for 100% depletion
η_{eff}	effective asthenospheric viscosity
ξ	dehydration stiffening coefficient
φ	porosity (i.e., melt content)
φ_C	critical porosity

small thermal perturbations (~3 K). SSC manifests itself in convection rolls aligned by plate motion with a spacing of ~200 km. Subsequently, convection transports heat to the base of the lithosphere, which hence maintains a nearly constant thickness [*Davaille and Jaupart*, 1993; *Dumoulin et al.*, 2001].

[20] SSC removes the bottom of the DHL in downwelling sheets (Animation S1 in the auxiliary material and Figure 4a), and replaces it with warm and fertile peridotite.[1] Consequently, decompression melting starts in the upwelling limbs of SSC. The flow geometry causes melting anomalies to be elongated and aligned by plate motion. Degrees of melting are low ($F \approx 2\%$), because decompression is ultimately restricted by the thickness of the lithosphere. These low degrees of melting complicate volcanism, as melt extraction requires F to exceed the critical porosity set to $\varphi_C = 1\%$. In case A, surface volcanism is thus 2 Ma delayed and 3.5-fold less voluminous than melting (see dashed lines in Figures 5a and 5c).

[21] As soon as partial melting initiates, it creates intrinsic buoyancy due to melt retention and depletion of the residue [*Schutt and Lesher*, 2006], and this positive feedback (previously termed buoyant decompression melting, or BDM) fuels convection [*Tackley and Stevenson*, 1993; *Schmeling*, 2000; *Raddick et al.*, 2002; *Hernlund et al.*, 2008].

Auxiliary materials are available in the HTML. doi:10.1029/2009GC002386.

In all of our models, however, the thermal boundary layer instability (i.e., SSC) dominates BDM. That is, for typical horizontal thermal variations in the asthenosphere of 300°C between upwellings and downwellings of SSC, thermal density anomalies are fivefold stronger than compositional density anomalies (for $\varphi_C = 1\%$).

[22] Because of BDM and the progressive removal of the DHL, melt production rates progressively grow until reaching a maximum beneath a 35-Ma-old lithosphere. Hereinafter, melt production declines and finally ceases beneath a seafloor of age ~47 Ma. The duration of melting, corresponding to $\pm 2\sigma$ of the distribution of melt production over seafloor ages (Figure 5a), is ~13 Ma. Melt extraction and surface volcanism are predicted to already stop earlier (at ~43 Ma), as soon as the maximum degree of melting drops below $\varphi_C = 1\%$ (duration of volcanism ~10 Ma).

[23] Durations of melting and volcanism are controlled by asthenospheric cooling during SSC. The asthenosphere cools with time because cold sublithospheric material is drawn downward and entrained. This mechanism progressively reduces density differences between upwellings and downwellings and thus the vigor of SSC on increasing seafloor ages. Moreover, maximum depths and degrees of melting are directly affected by asthenospheric cooling. As soon as the maximum degree of melting drops below φ_C, melt retention fades with a negative feedback on BDM, and this ultimately forces termination of magma production.

3.1.2. Case B, With Compositional Rheology

[24] In cases that include the effects of dehydration stiffening and melt lubrication (i.e., with CRh), it becomes more difficult for SSC to erode the base of the DHL. The main reason is that prior MOR melting created a stiff and thus resisting DHL (Figures 3b and 3d). As SSC melting requires erosion at the base of the DHL, it calls for relatively low η_{eff}. To compare cases A and B such that they yield similar melt production rates (see dashed lines in Figure 5), we use $\eta_{eff} = 2 \times 10^{18}$ Pa s in case B (with CRh, $\xi = 40$), which is 8 times less than in case A. The other parameters are unchanged.

[25] In reference case B, SSC first develops beneath a ~24 Ma old seafloor, which is ~2 Ma younger than in case A. The geometry of convec-

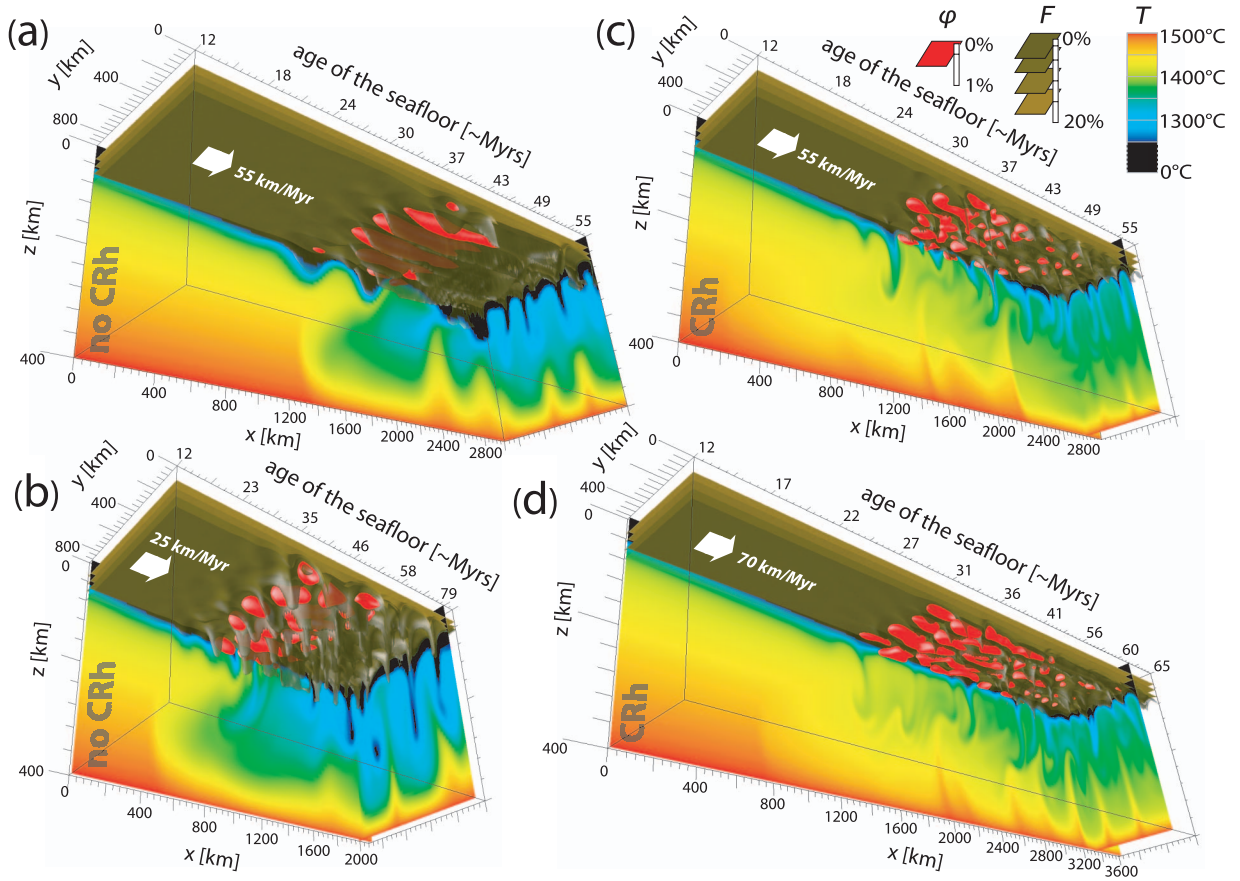

Figure 4. Isosurfaces of melt content (0.25%) and depletion (1.5%, 5%, 10%, and 15%), as well as cross sections of the temperature field are shown for (a and b) two cases without CRh and (c and d) two cases with CRh. Plate velocities v_{eff} are 55 km/Ma (Figures 4a and 4c), 25 km/Ma (Figure 4b), and 70 km/Ma (Figure 4d), as denoted by white numbers. The pattern of melting varies between cases with elongated anomalies (Figures 4a and 4d) and others with predominantly isometric anomalies (Figures 4b and 4c). The first (Figures 4a and 4d) are caused by sheet-like upwellings (i.e., convection rolls), and the latter (Figures 4b and 4c) are caused by point-like upwellings (i.e., hexagonal convection). The transition plate velocity between these two regimes is larger with CRh (~60 km/Ma) than without (~30 km/Ma). Furthermore, cases with CRh display weaker asthenospheric cooling due to SSC than cases without CRh for the same v_{eff} (see bluish/greenish colors in Figures 4a and 4c).

tion is dominated by hexagonal convection cells instead of convection rolls, resulting in almost isometric melt pockets above point-like upwellings (Animation S2 and Figure 4c). Melt production already starts at a seafloor age of ~27 Ma and rapidly reaches its maximum at a seafloor age of ~31 Ma. Compared to case A, melt production declines relatively slowly and continues to older seafloor ages of ~56 Ma (duration of melt production: ~25 Ma). As for case A, volcanism begins ~2 Ma later than melting. Because of a limited penetration of upwellings into the stiff DHL, the degrees of melting are smaller with CRh than without. Therefore, (1) the amount of magma extracted to the surface is fivefold lower than in case A and (2) the surface volcanism lasts only slightly longer even though melting endures almost twice as long (dashed lines in Figures 5b and 5d).

[26] Longer durations of melting and volcanism are caused by slower asthenospheric cooling in case B (Figure 4). First, slower cooling is due to that only the deepest portions of the thermal boundary layer (with sufficiently low η) are eroded by SSC with CRh and therefore the downwellings that cool the asthenosphere are warmer with CRh than without. Second, downwellings contain stiff harzburgite therefore tending to be only sluggishly mixed into the asthenosphere. Such a slow asthenospheric cooling allows long-term supply of warm peridotite to the melting zone, which results in longer durations of melting, and in an asymmetric distribution of melting over seafloor ages (Figure 5b).

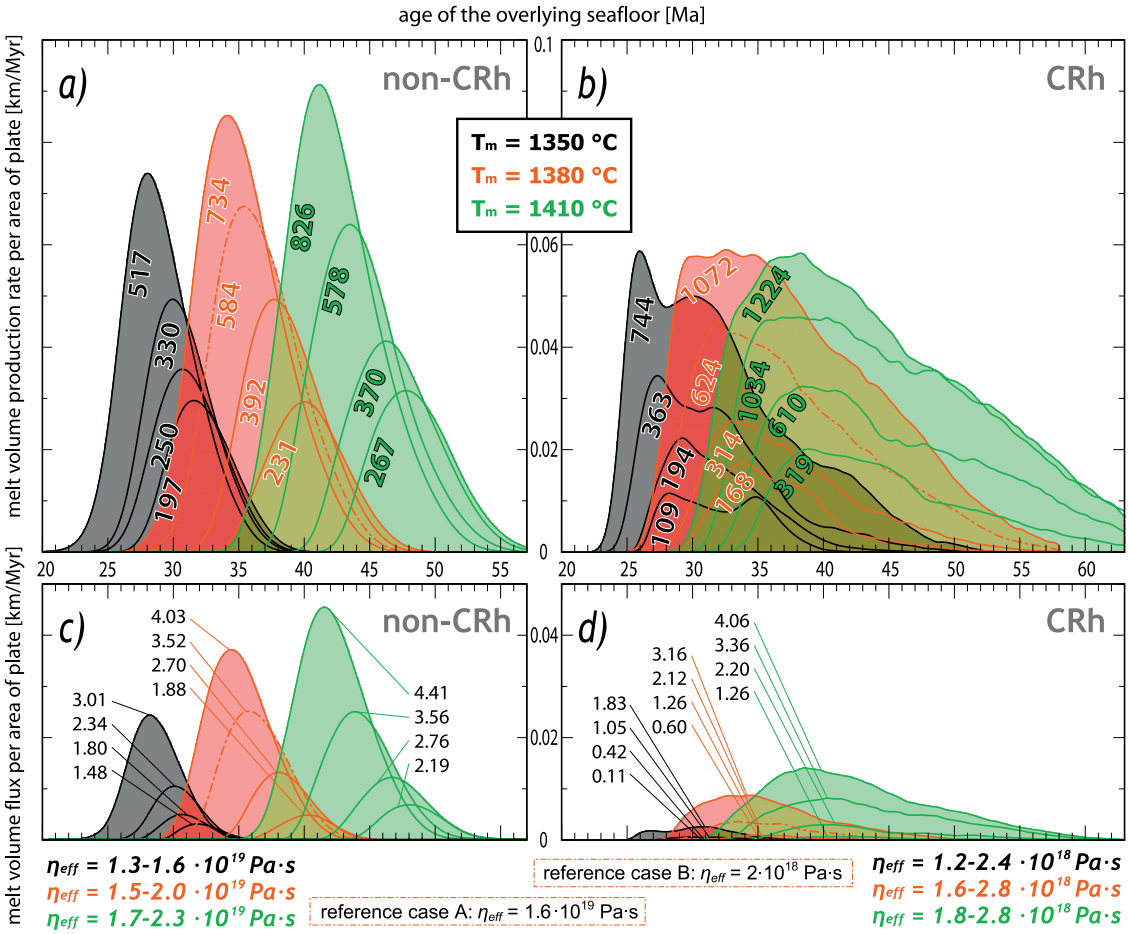

Figure 5. (a and b) The distribution of melt production over seafloor ages for diverse T_m (different colors) and various η_{eff} (different lines of the same color) without CRh ($\xi = 1$) and with CRh ($\xi = 40$). Each curve displays the melt production rate (Figures 5a and 5b) averaged along-strike of the plate at a certain age. The dash-dotted lines represent the reference cases A and B (see section 3.1). Melt volumes are most sensitive to η_{eff}, whereas seafloor ages during melting are most sensitive to T_m. The area beneath each curve is translated into a melt column height averaged over the full width of the plate, and the numbers in Figures 5a and 5b represent this height (m). (c and d) The distribution of extracted melt volume flux over seafloor ages for the same models. Numbers denote the height of virtual volcanoes (km) assuming that the cumulative amount of extracted melt (i.e., the area beneath the bottom curves) is redistributed into conical seamounts with a slope of 10° and a spacing of 100 km. Cases shown are identified in Figure S1; results of cases A and 43–52 were already published by *Ballmer et al.* [2007].

3.2. Mechanisms Controlling the Onset Age and Geometry of SSC

[27] SSC spontaneously evolves beneath mature oceanic lithosphere [*Richter*, 1973]. With increasing age of the lithosphere, the cold thermal boundary layer (TBL) below the oceanic plate thickens because of conductive cooling. The shallowest portion of the TBL behaves rigidly and only the lower warmer portion of the TBL has the ability to become gravitationally instable because of the temperature contrast across it δT_{TBL} [e.g., *van Hunen and Zhong*, 2006]. While thermal conduction is sufficient to dampen convective instability near the base of young and thin lithosphere, SSC develops as soon as the convectible TBL exceeds a critical thickness ($d_{TBL} > d_{crit}$) [*Parsons and McKenzie*, 1978]. The critical thickness d_{crit} can be derived from a local critical Rayleigh number:

$$\frac{\alpha \delta T_{TBL} \rho_0 g d_{crit}^3}{\kappa \eta_{eff}} = Ra_{crit} \tag{11}$$

$$\Leftrightarrow d_{crit} = \left(\frac{Ra_{crit} \kappa \eta_{eff}}{\alpha \delta T_{TBL} \rho_0 g} \right)^{1/3}. \tag{12}$$

[28] On the right-hand side of equation (12), η_{eff} is likely to be the most crucial parameter to define d_{crit} (Ra_{crit} is a constant for a given geometry).

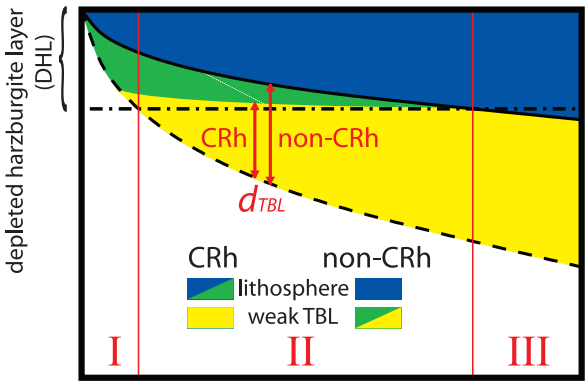

Figure 6. Possible regimes for SSC with and without CRh. Colors (nonwhite) represent the TBL thickening away from the MOR. Blue (and green) areas indicate the rheological lithosphere without CRh (with CRh, respectively). Yellow (and green) areas denote the convectible TBL with CRh (without CRh, respectively). In regimes I and II, the convectible TBL maintains a greater thickness d_{TBL} without CRh than with CRh. However, once established, the convectible TBL grows more rapidly with CRh in regime II. In regime III, the thickness of the lithosphere exceeds that of the DHL, and therefore, d_{TBL} is equivalent both with and without CRh.

Hence, the onset age of SSC (lithospheric age at which d_{TBL} exceeds d_{crit}) ultimately depends on η_{eff}, and on the vertical viscosity profile that controls, how d_{TBL} grows with age [*Conrad and Molnar*, 1999; *Korenaga and Jordan*, 2003]. With purely *T*-dependent rheology, d_{TBL} simply grows proportional to the square root of age as controlled by thermal conduction alone (Figure 6).

[29] Compositionally dependent rheology (CRh), however, severely inhibits SSC beneath younger seafloor, because for a long time of the cooling history of the TBL, the thickness of the stiff DHL exceeds that of the TBL [*Lee et al.*, 2005]. The thickness of the convectible TBL d_{TBL} thus remains smaller with CRh up to a significant plate age (regimes I and II in Figure 6). Because of this effect, smaller values of η_{eff} are required to maintain the same onset ages of SSC as without CRh. Only beneath sufficiently old seafloor, when the lithosphere is thicker than the DHL, the difference between CRh and no-CRh in terms of onset age dependence on η_{eff} vanishes (regime III in Figure 6).

[30] In addition, compositional density stratification further tends to stabilize the DHL [*Zaranek and Parmentier*, 2004]. Depletion and the related positive density anomaly increase upward within the DHL (Figure 3) providing a stable stratification that delays SSC. As the thickness of the convectible TBL and thus the compositional density anomaly across it are smaller with CRh than without, the effect of density stratification on onset ages is less important. In all models, we locate the onset age of SSC, where the vertical velocity in 100 km depth averaged over time first exceeds a certain threshold relative to the background vertical flow.

[31] After its onset, SSC self-organizes as "Richter" rolls aligned with the direction of absolute plate motion (Figure 1). This geometry is favored in order to minimize the interaction of SSC with the background large-scale flow from plate tectonics [*Richter*, 1973]. In contrast, hexagonal cells are the preferred pattern of convection without background flow [*Oliver and Booker*, 1983]. In our calculations without CRh, the plate velocity v_{trans} that separates these two regimes is about ~30 km/Ma (Figure 4a versus Figure 4c). For v_{eff} smaller than v_{trans}, hexagonal convection dominates in the shallow asthenosphere, because shear imposed by background flow is smaller than that induced by SSC itself. Otherwise, Richter rolls dominate.

[32] However, v_{trans} is larger (~60 km/Ma) with CRh than without comparing cases with similar onset ages (Figure 4b versus Figure 4d and Animation S2 versus Animation S3). Consequently, the style of convection at intermediate plate velocities (i.e., $v_{eff} \approx 30-60$ km/Ma) is dominated by cells with CRh and by rolls without. With CRh, the shearing by SSC is more vigorous (because of lower η_{eff}) and the shearing from plate motion preferentially concentrates below the stiff DHL, which is deeper than in cases without CRh. These two factors augment the impact of shearing associated with SSC compared to that associated with plate motion near the base of the lithosphere (where SSC first develops), and thus tend to promote cellular convection patterns for CRh [cf. *Marquart*, 2001].

3.3. Physics of Melting and Volcanism Related to SSC

[33] Figures 5, 7, and 8 show magma production rates (Figures 5a, 5b, 7a, 7c, 8a, and 8c) and melt extraction rates (Figures 5c, 5d, 7b, 7d, 8b, and 8d) over seafloor ages. The area beneath each curve in frames a/b represents the cumulative volume of magma *M* produced per km of plate (perpendicular to plate motion) during SSC melting (see denoted

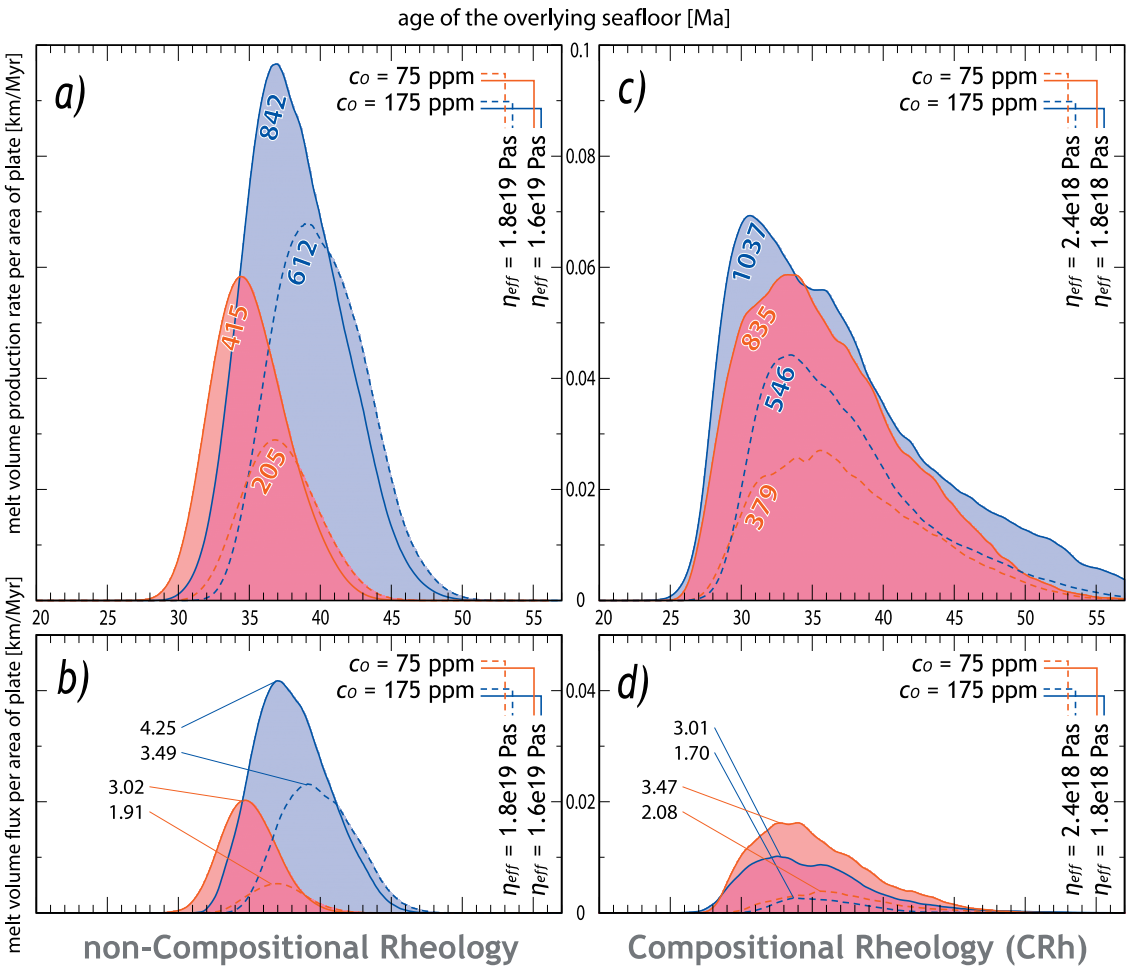

Figure 7. Same as Figure 5 in the parameter space c_O versus η_{eff} (a and b) without CRh and (c and d) with CRh.

numbers), and in frames c/d, it represents the cumulative volume of extracted melt (i.e., volcanism) per km of plate. SSC melting typically occurs at 80–100 km depth beneath seafloor of ages ~20 to ~60 Ma for models with η_{eff} on the lower bound of realistic values for the oceanic asthenosphere. Figures 5a, 5b, 7a, 7c, and 8a elucidate that melt production rates strongly increase with only small decreases in η_{eff}. This behavior is caused by the following two mechanisms. First, decreasing η_{eff} yields earlier onset ages of SSC [*Richter and Parsons*, 1975] therefore reducing the thickness of the rigid lithosphere with a positive effect on the maximum degree of melting. Second, decreasing η_{eff} fuels the vigor of convection with a positive effect on peridotite fluxes through the melting zone.

[34] We investigate the effects of the sensitivity of rheology to melt and water content by varying the water depletion stiffening coefficient ξ between the end-members 1 and 100 (default: 40 for CRh). In contrast, we keep the melt lubrication exponent ζ fixed. The most important implication of increasing ξ is that partial melting from SSC requires lower η_{eff} for higher ξ (Figure 8a). Decreasing η_{eff} offsets the most important drawbacks of a stiff DHL on SSC melting: delay of SSC (see section 3.2), and limitation of degrees of melting (see section 3.1.2). But as the latter has a more restrictive effect on melting than the former, M is less for higher ξ comparing cases with a similar onset age of SSC (Figure 8a).

[35] Since η_{eff} controls both the amount and the degree of melting, it has a strong impact on the flux of surface volcanism. Melt is extractable to the surface only where maximum degrees of melting exceed φ_C, so (1) small decreases of η_{eff} are sufficient to significantly increase the heights of predicted seamounts (see numbers denoted in Figures 5d, 7d, 8b, and 8d) and (2) durations of

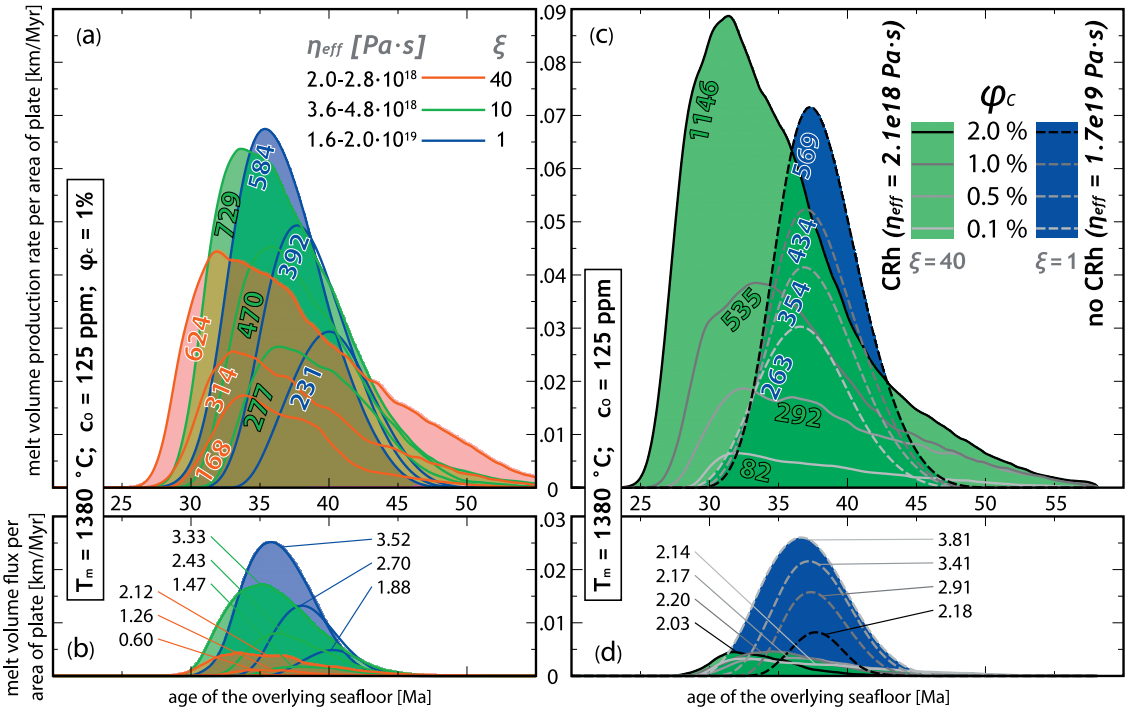

Figure 8. (a) Melt production rates and (b) melt extraction rates over seafloor ages for different η_{eff} and water depletion stiffening coefficients ξ. Without CRh (i.e., ξ = 1), the durations of melting and volcanism are relatively short and the distribution is symmetric. For larger ξ (i.e., CRh), durations are progressively longer and distributions progressively more asymmetric. The fraction of melt being extracted to the surface is relatively large without CRh and progressively smaller for $\xi > 1$. The onset ages of SSC and η_{eff} required for similar melt production rates are weakly negatively and strongly negatively correlated with ξ, respectively. (c) Melt production rates and (d) melt extraction rates over seafloor ages for different φ_C with and without CRh. The area beneath the curves represents cumulative magma volumes per Ma and per km of plate (produced and extracted, respectively). The volume of magma produced always positively correlates with φ_C (Figure 8c). In contrast, the volume of magma extracted negatively correlates with φ_C for non-CRh, whereas it is almost independent of φ_C for CRh (Figure 8d). Numbers denoted in all frames as described for Figure 5.

volcanism are greater for lower η_{eff}, although durations of melting are insensitive to η_{eff}.

[36] In sections 3.3.1–3.3.4, we investigate the effects of four important parameters ($\Delta\rho_F$, T_m, c_O, c_O, c_O, and φ_C) on onset ages of SSC, as well as on amounts and durations of melting and volcanism (Table S1). In each subsection, we commence with simple models neglecting CRh before turning to models with CRh. This enables us to isolate the effects of CRh. In section 3.3.5, we summarize the most robust predictions of this parameter study.

3.3.1. Stable Stratification Related to the DHL

[37] The intrinsic buoyancy of the DHL provides a stable layering of the upper mantle that delays convection [*Zaranek and Parmentier*, 2004]. The depletion of the harzburgite usually ranges from ~20% near the surface to a few percent at depths of 80–100 km (Figure 3a). The delay of SSC depends on the density increase with depletion $\Delta\rho_F$ as well as on the vertical density profile (i.e., the vertical depletion profile within the DHL), a profile that is influenced by T_m and c_O mostly (Figure 3a).

[38] We apply a default value of $\Delta\rho_F = -72.6$ kg/m^3, such as proposed by *Schutt and Lesher* [2006] for the relevant depths of SSC melting (80–100 km), although estimates ranging from −300 kg/m^3 to 0 kg/m^3 have been proposed. Figure 9a shows melt production over seafloor ages without CRh. We find that larger values of $\Delta\rho_F$ systematically delay SSC, and decrease M. As $\Delta\rho_F$ does neither affect the depth of the solidus nor dampen the vigor of SSC, its negative effect on M is caused by the delay of SSC alone. Accordingly, the effect of $\Delta\rho_F$ on M is small compared to that of η_{eff} as demonstrated by

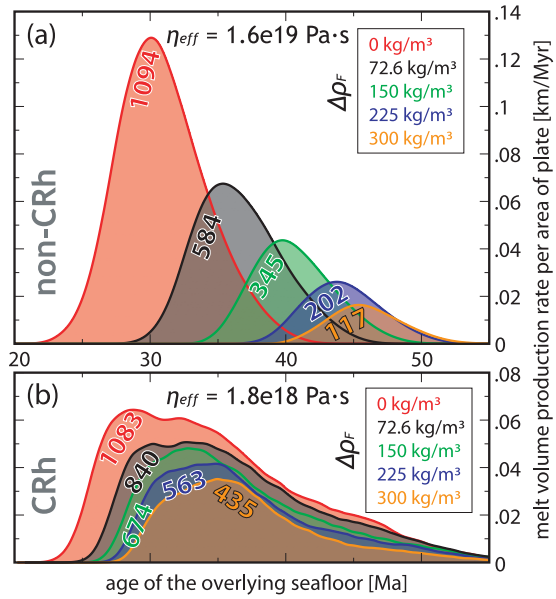

Figure 9. Melt production over seafloor ages for different $\Delta\rho_F$ (a) without and (b) with CRh. Numbers denoted as described for Figures 5a and 5b.

comparison of models with similar onset ages of SSC and with different pairs of $\Delta\rho_F$ and η_{eff} (e.g., cases 19 versus 50 without CRh, and cases 101 versus 103 with CRh; see Table S1).

[39] With CRh, total compositional density variation within the relatively thin convectible TBL (see Figure 6) is small, and therefore compositional density stratification has a relatively small impact on onset ages and on SSC melting. This finding is demonstrated by the small shifts in ages and volumes of SSC melting with varying $\Delta\rho_F$ as shown in Figure 9b.

3.3.2. Mantle Reference Temperature

[40] Figure 5 shows that higher T_m ultimately delay SSC and enhance melting. While the average upper mantle temperature is relatively well constrained, T_m may strongly vary spatially. In this study, we explore models with T_m on the upper bound of the range of realistic reference temperatures from 1350°C to 1410°C [*Herzberg et al.*, 2007]. First, T_m has a large influence on the solidus with higher values enabling deeper and more extensive SSC melting [*Katz et al.*, 2003]. Second, higher T_m also yields equally more extensive MOR melting, which gives rise to a thicker DHL (Figure 3a), and hence delays SSC with a negative feedback on the total melt production M. For no-CRh, the first effect however is more important than the second effect leaving with a positive correlation of M and T_m (Figure 5a).

[41] In contrast, our models with CRh show only a weak positive relation of the maximum magma production rate (Figure 5b) and the maximum degree of melting (not shown) to T_m. The effects of a deeper solidus are efficiently offset by the progressive restriction of decompression due to a thicker DHL for higher T_m. However, the time-integrated total melt production also depends on the duration of melting, which itself positively depends on onset age (and hence T_m) with CRh but less so without CRh (see section 3.3.5). The net effect of the relations of the maximum degree and the duration of melting with T_m is a positive correlation of M with T_m (Figure 5b).

3.3.3. Bulk Water Content

[42] In the simplified case without CRh, the effects of bulk water content c_O are similar to those of T_m: higher c_O also increases both the depth of the solidus and the thickness of the DHL. Therefore, onset ages of SSC, seafloor ages over which melting occurs, and total melt production M are all positively related to c_O (Figure 7). Exploring models with the full range of realistic bulk water contents (75–200 ppm) [*Hirth and Kohlstedt*, 1996] reveals that the effects of c_O (on onset ages and M) are smaller than those of T_m in the parameter range explored. Increasing c_O by 100 ppm approximately offsets decreasing T_m by 20°C (Figure 5a versus Figure 7a).

[43] In contrast, in models with CRh, onset ages of SSC melting are almost independent of c_O (Figure 7c). Bulk water content c_O influences both the thickness of the rheological lithosphere and the sharpness of the rheological boundary at its base (Figure 3c). These competing effects mostly compensate each other in terms of onset age. The maximum degree of melting, however, decreases with increasing c_O, because a certain degree of melting requires a thicker portion of the stiff DHL to be removed for increasing c_O (see Figure 3c). First, this behavior dampens the otherwise positive relation of M to c_O (Figure 7c). Second, it limits the depth range, over which the degree of melting exceeds the critical porosity, yielding a negative correlation of the amount of volcanism with c_O (Figure 7d).

3.3.4. Critical Porosity

[44] Partial melting due to SSC is supported by buoyant decompression melting (BDM, see

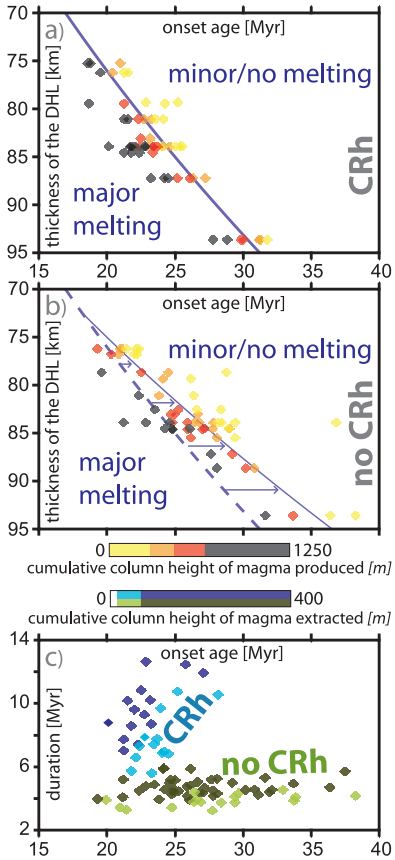

Figure 10. (a and b) Onset ages of SSC versus the depth at which an adiabatically decompressing parcel of peridotite reaches $F = 1\%$ for most of the models with minor or no melting (yellow and orange diamonds) and major melting (red and black diamonds). The depth of the boundary between the minor melting and major melting regimes (solid lines) scales linearly with the square root of onset age with CRh (Figure 10a), but it deviates from this scaling (dashed line) without CRh (Figure 10b). (c) The durations of volcanism versus onset ages of SSC for models without CRh (green) and with CRh (blue). Comparing models with a similar amount of volcanism (i.e., diamonds with the same color tone) reveals that durations of volcanism are sensitive to onset ages with CRh, whereas they are almost constant without CRh.

section 3.1.1). Typical density anomalies related to melt retention (5 kg/m^3 for 1% melt) are larger than those related to depletion (1.5–2.2 kg/m^3 for 2–3% depletion). Moreover, the downwelling limbs of SSC are inhibited by the compositional buoyancy of depleted harzburgite but not influenced by retained melt because it freezes before it sinks. Therefore, melt retention buoyancy dominates BDM, and the vigor of BDM scales with the maximum fraction of retainable melt (i.e., critical porosity φ_C). φ_C varies with volatile content and shear stress [*Stevenson*, 1989; *Faul*, 2001; *Katz et al.*, 2006], but in a simplified approach we apply a constant φ_C in each model [*Schmeling*, 2006]. We vary this parameter between the end-members of 0.1% and 2% with a default value of 1% [*Faul*, 2001; *Stracke et al.*, 2006].

[45] Our results without CRh show that increasing φ_C increases melt production rates but decreases melt extraction rates (Figures 8c and 8d). The positive influence of φ_C on melt production is due to the combination of three, partly counteracting effects: (1) as high values of φ_C encompass a more vigorous BDM, SSC penetrates deeper into the lithosphere resulting in higher degrees of melting. Furthermore, (2) since water separates later from the solid for high values of φ_C, solidus temperatures for moderately low degrees of melting are reduced (Figure 2). Finally, (3) this retarded water separation also enhances depletion at a given depth from prior MOR melting (Figure 3c). Additional simulations (with $\Delta\rho_\varphi = 0$) reveal that more vigorous BDM (effect 1) has a larger effect on M (i.e., melt production) than slower separation of water (effect 2). Effect 3 causes a weak positive correlation of onset ages with φ_C that, however, only slightly offsets the first two effects in terms of M. Despite the overall positive relation between the amount of melting (i.e., M) and φ_C, the total amounts and durations of surface volcanism are negatively correlated with φ_C (Figure 8d), which indicates that larger φ_C has the dominating effect of reducing the amount of extractable melt (see section 3.3.3).

[46] While the effects of reducing φ_C on M are similar for both CRh and no-CRh, reducing φ_C is insufficient to boost volcanism for CRh (unlike for no-CRh). Degrees of decompression melting are progressively restricted for lower φ_C because lower φ_C creates a progressively thicker rheological lithosphere (Figure 3d) due to the more effective dehydration during MOR melting. This thicker lithosphere reduces the degrees of melting and M; however, because volcanism is promoted by reduced φ_C, eruption flux does not sense the reduction in melting and thus is insensitive to φ_C (Figure 8d).

3.3.5. Conclusion of the Parameter Study

[47] Figures 10a and 10b display the "effective thickness of the DHL" (see Figure 10 caption) versus onset age of SSC for each model with (ξ = 40) and without (ξ = 1) CRh, respectively. The

models plot within two regimes: one regime displays minor or no melting (orange and yellow diamonds in Figure 10), and another regime displays major melting (black and red diamonds). The major melting regime is favored by early onset ages or, at intermediate onset ages, by smaller "effective thicknesses of the DHL." For cases with CRh, the "effective thickness of the DHL" at the boundary between the two regimes linearly scales with the square root of onset age (i.e., with the thickness of the TBL). However, the scaling law differs for the cases without CRh (see arrows in Figure 10b): for large "effective thicknesses of the DHL" major melting appears to be possible later onset ages than with CRh. Without CRh, penetration of SSC (once it is established) into a thick DHL is only relatively mildly restricted by density stratification (compared to a severe restriction by rheological stratification with CRh). Therefore, even cases with relatively late onset ages display major SSC melting without CRh.

[48] Figure 10c shows the duration of volcanism plotted against the onset age of SSC for the same suite of models. Comparing cases with a similar amount of volcanism, the durations of volcanism are long and sensitive to onset age with CRh, whereas they are short and almost independent of onset age without CRh. Long durations with CRh are caused by slow asthenospheric cooling due to the effects of a stiff DHL (see section 3.1.2). Specifically, a thicker DHL and higher η_{eff} both delay SSC and reduce the cool material flux from the base of the lithosphere to the asthenosphere. Thus later onset ages correlate with slower asthenospheric cooling and longer durations of melting. In contrast, the cool material flux to the asthenosphere is not restricted by stiffening within the DHL in cases without CRh. This accounts for uniformly fast asthenospheric cooling thus causing short and almost constant durations of volcanism (Figure 10c).

[49] To summarize the most important predictions of the models with CRh, the duration of surface volcanism from SSC and its total amount increase with decreasing φ_C or η_{eff}, and with increasing T_m. Furthermore, surface volcanism increases with higher T_m and η_{eff}, with the effect of T_m being greatest. Total crustal thicknesses of individual volcanoes are predicted to exceed 1 km for a broad range of the parameter space (see numbers denoted in Figures 5d, 7d, and 8d). Finally, the simplification of neglecting CRh is insufficient to capture many of the important effects of CRh (sections 3.3.1–3.3.4 and Figure 10).

4. Discussion and Conclusions

4.1. Discussion of the Modeling Results

[50] SSC is capable of generating volcanism simply by overturning the thermal and compositional stratification of the upper mantle. Our models consider a petrological spectrum from lherzolites to harzburgites plus some hydrous fluid. Prediction of realistic geochemistry of ocean island basalts would require, however, more complicated lithologies and fluid compositions, including CO_2 [*Niu and O'Hara*, 2003; *Sobolev et al.*, 2007; *Dasgupta et al.*, 2007; *Pilet et al.*, 2008].

[51] Fertile lithologies may survive MOR melting at depths greater than 100–150 km (e.g., enriched peridotite or pyroxenite [cf. *Ito and Mahoney*, 2005, and references therein]), or may be incorporated into the oceanic lithosphere (i.e., metasomatized hornblendite veins [*Niu and O'Hara*, 2003; *Pilet et al.*, 2008]). Deep sources of fertile lithologies may be stirred up by SSC, and metasomatized veins may be either pulled down into warmer levels by SSC itself or reheated by ascending SSC-derived magmas. Since these processes enable extensive melting, and since only low-degree melting of peridotites occurs, the geochemistry of SSC-derived magmas is likely to be dominated by the most fusible, and thus perhaps geochemically enriched sources (M. D. Ballmer et al., Small-scale sublithospheric convection reconciles geochemistry and geochronology of "superplume" volcanism in the western and South Pacific, submitted to *Earth and Planetary Science Letters*, 2009). Since the current models do not consider such fertile materials, the melt volumes presented here should be regarded as lower bounds.

[52] Our calculations predict that SSC melting with CRh requires early onset ages (i.e., 20–35 Ma) and therefore effective viscosities of $\eta_{eff} < 3 \times 10^{18}$ Pa s, which are likely to be on the lower end of realistic values for the oceanic asthenosphere [cf. *Cadek and Fleitout*, 2003]. However, accounting for lateral density heterogeneity (compositional or thermal) would locally reduce onset ages of SSC [*Huang et al.*, 2003; *Dumoulin et al.*, 2005, 2008] compared to our homogeneous models (Figure 1). An example calculation with a small along-strike thermal heterogeneity (of just 10 K) with CRh reveals that $\eta_{eff} \approx 4 \times 10^{18}$ Pa s is sufficiently low for triggering early SSC with associated magma

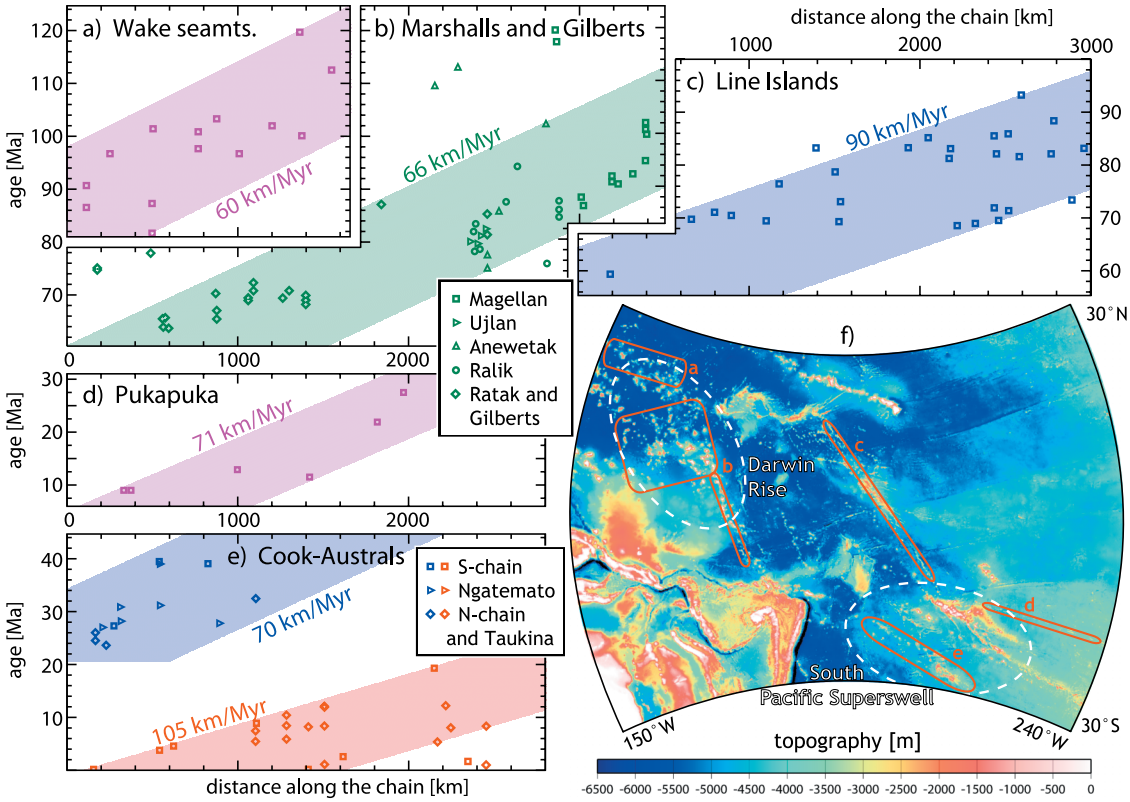

Figure 11. Ages collected at (a) the Wake seamounts, (b) the Marshalls, (c) the Line Islands, (d) the Pukapuka ridges, and (e) the Cook-Australs plot within fields in age-distance space of widths 1500 km (Figures 11a, 11b, and 11e), 2000 km (Figure 11c), and 1000 km (Figure 11d). This behavior is consistent with volcanism formed on the Pacific Plate overriding a quasi-stationary elongated magma source. In Figures 11b and 11e distances are obtained by projecting the locations of the seamounts of each of the 5 and 2 lineaments (see legends), respectively, on top of each other (with a projection axis parallel to the lineaments). (f) Positions of the volcano chains on the Pacific Plate. In order to avoid introducing additional scattering, we take ages only from a limited number of reliable sources: Figures 11a and 11b are from *Koppers et al.* [2003, 2007]; Figure 11c is from *Davis et al.* [2002, and references therein]; Figure 11d is from *Sandwell et al.* [1995]; and Figure 11e is from *Chauvel et al.* [1997], *McNutt et al.* [1997], *Bonneville et al.* [2006], and some other sources [*Duncan and McDougall*, 1976; *Turner and Jarrard*, 1982] for seamounts without more recent analyses available.

generation. Since stronger density heterogeneity than that is expected to exist throughout the upper mantle [*Phipps Morgan and Morgan*, 1999; *Herzberg et al.*, 2007], we believe that realistic η_{eff} of 5×10^{18} perhaps up to 10^{19} Pa s are sufficient for significant volcanism from SSC.

[53] A key prediction is that individual melting zones due to SSC are elongated and parallel to plate motion (previously referred to as a "hot line" [*Bonatti and Harrison*, 1976]). These melting zones each emerge above a single sheet-like upwelling of SSC (in the regime of convection rolls as for plate velocity $\geq$60 km/Ma). We predict durations of major melting of $\sim$25 Ma for our more realistic models with CRh. The corresponding time scale of volcanism is in the range of 10–20 Ma. On the fast Pacific plate, these time scales correspond to an elongation of the zones of melting and of volcanism of up to $\sim$2000 km and of 700–1600 km, respectively (taking 70–80 km/Ma [cf. *Schellart et al.*, 2008, and references therein]). However, these estimates are lower bounds, as our calculations neglect radiogenic heating, a process that slows asthenospheric cooling [*Huang and Zhong*, 2005; *Afonso et al.*, 2008].

[54] Age-distance relationships of a volcanic chain formed on a plate moving over such an elongate melting anomaly (hot line) are not expected to be linear. Ages are rather predicted to plot within a broad field in age-distance space bound by two linear trends with equal slope that roughly corresponding to plate velocity (Figure 11) and separated in time by duration of SSC melting.

Correspondingly, the width of the field on the distance axis corresponds to the length scale of volcanism due to SSC (i.e., 700 to >1600 km). This broad swath in age-distance is predicted for a "hot line" of volcanism [*Bonatti and Harrison*, 1976], in contrast to a more narrow trend in age-distance predicted for localized hot spots. Another important prediction of our models is that volcanism caused by SSC emerges on seafloor of intermediate ages (20–60 Ma).

[55] These predictions may give an explanation for previously enigmatic ages along volcano chains on the Pacific Plate. Radiometric ages from the Marshalls, Cook-Australs, Line Islands, Wake seamounts, the Gilbert ridges and the Pukapuka ridge do not follow the most fundamental predictions of hot spot theory. All these examples were formed above (or at the edge) of the South Pacific Superswell (SPSS) or its Cretaceous precursor, the Darwin Rise, which both are likely regions with anomalously high temperature and heterogeneous composition, maybe underlain by a "superplume" [*Staudigel et al.*, 1991; *McNutt*, 1998]. SSC may evolve at the edges of a low-viscosity superplume spreading within the higher-viscosity mantle or above its roof in case it stalls below the transition zone [*Griffiths and Campbell*, 1991]. Indeed, high temperatures and low viscosities in the SW Pacific asthenosphere [*Staudigel et al.*, 1991; *Cadek and Fleitout*, 2003] settle the most important requirements to drive vigorous SSC [*Richter*, 1973]. This scenario is in accord with the interpretations from geochemical observations at some of the above mentioned volcano chains for mixing between enriched lower mantle (from the superplume), depleted upper mantle, and the oceanic lithosphere [*Janney and Castillo*, 1999; *Janney et al.*, 2000]. Regarding these tight constraints, we believe that SSC is a subordinate mechanism to produce volcanism in the northern Pacific or in other ocean basins, where such a large-scale temperature or compositional anomaly is not present.

4.2. Application to Volcano Chains in the Pacific

4.2.1. Marshall Islands and Gilbert Ridge

[56] The Marshall Islands consist of multiple parallel seamount trails (i.e., Magellan, Ujlan, Anewetak, Ralik and Ratak) with a lateral spacing of 200–300 km. They are located on the Darwin Rise, the Cretaceous precursor of the SPSS [*Smith et al.*, 1989; *Staudigel et al.*, 1991] with submerged volcanoes (atolls and guyots) that once rose 4–5 km above the seafloor. They erupted on seafloor of ages 50–90 Ma displaying irregular patterns of geographic age progressions along each individual seamount trail [*Koppers et al.*, 2003]. Apparently coeval volcanism spans distances of ~1000 km, a behavior that is best documented for Magellan, Ralik, and Ratak trails. Most of the sample ages including even those of the Gilbert ridge [*Koppers et al.*, 2007], the southern continuation of the Ratak trail, plot within a field of width ~1500 km (Figure 11b). The slope of that field and the orientation of the trails agree well with Pacific plate motion during the Emperor stage pole (62–74 km/Ma [cf. *Koppers et al.*, 2007, and references therein]).

[57] The large distance spans of apparently coeval volcanism at the Marshall Islands and Gilbert ridges are difficult to reconcile with a hot spot, channelized return flow, or lithospheric cracking. SSC better accounts for sample ages plotting in an age-distance field of width ~1500 km. The geographic spacing between the seamount trails is in accord with the predictions of the SSC hypothesis, as well. Partial melting in abundant fertile lithologies may account for seafloor ages during volcanism beyond the upper range of our predictions (i.e., 50–90 Ma) enabling melting beneath an older and thicker lithosphere than predicted by our simulations (Ballmer et al., submitted manuscript, 2009). As consistent with this hypothesis, geochemistry of basalts from the Marshalls stretch out between endmembers "HIMU" and "EMI" [*Koppers et al.*, 2003; *Konter et al.*, 2008].

4.2.2. Pukapuka Ridges

[58] The Pukapuka ridges are a series of en echelon ridges with a total length of ~2000 km between the eastern edge of the SPSS and the Rano-Rahi seamount field [e.g., *Sandwell et al.*, 1995]. It lies on seafloor that is 10–30 Ma older than the individual volcanoes, and the volcano heights are ~2 km [*Lynch*, 1999]. Volcano ages along the ridge do not follow a systematic trend (Figure 11d) consistent with an absolute plate motion of ~70 km/Ma [*Schellart et al.*, 2008, and references therein]. Pukapuka is accompanied with gravity and topography lineations of wavelength ~200 km [*Haxby and Weissel*, 1986; *Buck and Parmentier*, 1986], of which analysis reveals a buoyant mantle reservoir beneath Pukapuka [*Marquart et al.*, 1999] and neighboring ridges [*Harmon et al.*, 2006, 2007]. Furthermore, geochemical trends along Pukapuka suggest shallow mixing of an enriched reservoir from the west (i.e., the SPSS) with depleted peri-

dotites from the East Pacific Rise [*Janney et al.*, 2000].

[59] Geophysical and geochemical constraints are in concert with the SSC hypothesis. Geochronological data along the Pukapuka ridges is sparse but apparently inconsistent with hot spot theory [*Sandwell et al.*, 1995]. A systematic age-distance relationship of ~300 km/Ma has been put forward to be valid for the eastern part of the ridges but without providing a credible mechanism for such a fast age progression of the melting source (see section 1). Alternatively, sample ages may be explained by volcanism over a quasi-stationary melting zone of elongation ~1000 km from SSC (Figure 11d). This elongation on the lower bound of our model predictions, together with the observed volcano heights and seafloor ages during volcanism (10–30 Ma) are generally consistent with cases with low T_m. Slightly earlier onset ages of SSC than predicted from our models may arise from lateral density heterogeneity [*Huang et al.*, 2003; *Dumoulin et al.*, 2008]. Alternatively, colder mantle temperatures beneath the East Pacific Rise than beneath the SPSS such as proposed by *Hillier and Watts* [2004] likely give rise to an unusually thin DHL that allows early SSC. Unusually thin elastic thicknesses in this region [*Goodwillie*, 1995] supports this scenario. However, our models (that exclude the MOR) are unable to explain volcanism at the eastern edge of Pukapuka and within the Rano-Rahi seamount field, which have both been formed in direct proximity of the MOR.

4.2.3. Cook-Austral Islands

[60] The Cook-Austral double chain (S and N branch, spaced ~250 km) is located above the southern edge of the South Pacific Superplume and displays a complicated history of multiple episodes of volcanism. Ages of samples plot within two age-distance fields of width ~1500 km distinguishing two major episodes of volcanism (Figure 11e). An early episode of volcanism (at about 40–20 Ma) formed three parallel seamount chains with an internal spacing of ~150 km at the eastern edge of the Australs on young seafloor (10–30 Ma): Taukina, Ngatemato, and the continuation of the S branch. Moreover, most of the volume of many of the large (up to 5 km high) volcanoes in the two main branches already erupted during this episode with a topping formed later in time [*McNutt et al.*, 1997]. The recent episode of volcanism (<20 Ma) emerged on younger seafloor of ages 50–90 Ma along the two main branches.

[61] To fit within the hot spot theory, the recent volcanic episode and its complex age-distance patterns require many short-lived hot spots (i.e., at least three [*Bonneville et al.*, 2002, 2006] or substantially more than that [*McNutt et al.*, 1997; *Clouard and Gerbault*, 2008]). Coeval volcanism is separated by up to ~1200 km, and individual edifices display successive volcanic stages with intermittent quiescence of 4–11 Ma [*Turner and Jarrard*, 1982; *Bonneville et al.*, 2002, 2006]. Including earlier ages (>20 Ma) increases the number of required hot spots to ~8 [*Clouard and Bonneville*, 2005]. Mechanisms proposed for multiple hot spots include secondary short-lived plumelets rising from the top of the South Pacific Superplume in the transition zone [*Davaille*, 1999], or a plume forest [*Schubert et al.*, 2004]. However, such an interpretation of the hot spot theory is complex and therefore perhaps farfetched. Furthermore, the recent episode of volcanism (<20 Ma) shows an overall age-distance slope of ~110 km/Ma [e.g., *Chauvel et al.*, 1997], a rate that is significantly faster than absolute Pacific plate motion (70–80 km/Ma [cf. *Schellart et al.*, 2008, and references therein]).

[62] We rather propose that volcanic episodes (<40 Ma) forming the Cook-Austral dual chain are fed by two parallel hot lines (of length ~1500 km) as caused by SSC. Such a situation naturally creates large distances of apparently coeval volcanism (Figure 11e) and the observed spacing of the lineaments. For the earlier episode of volcanism (40–20 Ma), the trend in age versus distance (~70 km/Ma) and seafloor ages during volcanism are fully consistent with our predictions as well.

[63] That SSC volcanism reemerges on mature seafloor (50–90 Ma) during the recent episode (<20 Ma) may be explained by the reactivation of SSC due to the introduction of a combination of hotter and abundant fertile mantle lithologies in the mantle below the SPSS [*Konter et al.*, 2008] perhaps related to the superplume. That the age-distance trend of the recent episode (~105 km/Ma) is slightly faster than absolute plate motion would require some form of eastward propagation of the hot line. Generally, propagation of a hot line is a realistic process that is controlled by the sensitivity of the onset age of SSC to lithospheric thickness and mantle viscosity.

4.2.4. Wake Seamounts

[64] Also for the Wake seamounts, SSC appears to be more consistent with observations than hot spot

theory. The Wakes are two parallel lineaments of guyots (spacing ~250 km) located on the northern edge of the Darwin Rise. They erupted at 80–120 Ma on seafloor of ages 30–60 Ma. Ages collected along the Wake seamounts tend to increase with distance along the chain (with a general age-distance trend of ~60 km/Ma) but scatter substantially (Figure 11a). It is unclear, whether this age-distance trend is equal to or faster than absolute Pacific plate motion in the Jurassic, but reliable ages make it obvious that coeval volcanism has spanned a distance ~1500 km [*Koppers et al.*, 2003].

4.2.5. Line Islands

[65] Volcanoes along the Line Islands spatially and temporally developed between volcanism at the SPSS and at the Darwin Rise (likely associated with a pulse of the superplume between 90 Ma and 30 Ma [*Adam and Bonneville*, 2005]). Before being eroded, volcanoes rose >4 km above the seafloor, a size similar to those at the Marshall or Cook-Austral Islands. They erupted during two major episodes (at 68–73 Ma, and at 81–86 Ma) on seafloor with ages 30–55 Ma [*Davis et al.*, 2002]. Volcanism emerged synchronously at least over the full length of the northern part of the chain (~2000 km). Conclusions on the ages of its southern part remain vague as reliable geochronologic data is unavailable [*Davis et al.*, 2002].

[66] The above constraints are consistent with a volcano chain being formed over a hot line, such as caused by SSC. Volcano sizes, and ages of the seafloor during volcanism (30–55 Ma) are consistent with our model predictions for high T_m, but the observed length scale of volcanism (~2000 km, see Figure 11c) is somewhat too large to fit predictions (~1500 km). However, predicted length scales are lower bounds because of negligence of radiogenic heating in our models (see section 4.1). Moreover, small volume volcanism derived from fertile mantle lithologies may extend on older seafloor than predicted for peridotite-derived volcanism with sampling typically being biased toward these late stages of volcanism.

[67] Our data analysis (sections 4.2.1–4.2.5) shows that SSC is a likely mechanism to explain non–hot spot intraplate volcanism. This work accentuates the need for more reliable geochronologic data to further test our predictions as well as to potentially identify more non–hot spot ridges.

4.3. Conclusions

[68] The most important conclusions of this study are the following.

[69] 1. Thermally driven SSC tends to occur near and displace the bottom of the DHL replacing it with fertile peridotite. Consequently, SSC generates decompression melting and spawns volcanism. This behavior is predicted to spontaneously evolve from a simple cooling oceanic lithosphere and does not presume any large thermochemical anomalies (e.g., plumes). The sole requirement is a sufficiently low asthenospheric viscosity.

[70] 2. A steep rheological gradient at the base of the intrinsically stiff DHL formed by extraction of water during MOR melting diminishes the thickness of the convectible thermal boundary layer. Therefore, SSC is retarded, and its onset ages are coupled to the thickness of the DHL.

[71] 3. The stiffness of the DHL complicates its removal and subsequent SSC melting, but it also prevents shallow (i.e., cool) layers from participating in SSC thus retarding asthenospheric cooling. Consequently, the duration of SSC melting is prolonged (to ~25 Ma). As the DHL is thicker for higher T_m, durations positively relate to T_m. The presence of a stiff DHL reduces the degree of partial melting compared to cases neglecting the intrinsic stiffness of the DHL.

[72] 4. Our numerical models predict SSC melting to emerge beneath seafloor of ages ~20 to ~60 Ma for $\eta_{eff} \leq 3 \times 10^{18}$ Pa s. The average age of the seafloor over which volcanism occurs predominantly scales with T_m. The amount of magma production scales with the onset age of SSC and with the depth of the solidus. Onset ages of SSC decrease with higher η_{eff} and φ_C, and increase with higher T_m.

[73] 5. Models predict volcanism to last 10–20 Ma and thus reconcile longevity of individual volcanoes (10–20 Ma), and synchronous volcanic activity over 700–1600 km along individual ridges (for a Pacific-like plate motion of 70–80 km/Ma). Correspondingly, associated age-distance fields are parallel to plate motion with a finite width of 700–1600 km. However, they may also be oblique to plate motion in case the onset age of SSC is time-dependent. These predictions explain many observations at the Pukapuka ridges, Wake seamounts, Line Islands, Marshalls, Gilberts, and Cook-Austral Islands that appear to disagree with hot spot theory.

Acknowledgments

[74] We wish to thank Caroline Dumoulin and Harro Schmeling for their thorough and valuable reviews and P. van Keken for editorial handling and leading the fruitful review process. M. Ballmer was sponsored by SNF projects 20021-107995/1 and 20020-119922/1. G. Ito and T. Bianco were supported by NSF grants EAR-0040365 and EAR-0510482.

References

Adam, C., and A. Bonneville (2005), Extent of the South Pacific Superswell, *J. Geophys. Res.*, *110*, B09408, doi:10.1029/2004JB003465.

Afonso, C. A., S. Zlotnik, and M. Fernàndez (2008), Effects of compositional and rheological stratifications on small-scale convection under the oceans: Implications for the thickness of oceanic lithosphere and seafloor flattening, *Geophys. Res. Lett.*, *35*, L20308, doi:10.1029/2008GL035419.

Anderson, D. L. (2000), The thermal state of the upper mantle; no role for mantle plumes, *Geophys. Res. Lett.*, *27*, 3623–3626.

Anderson, D. L., and J. D. Bass (1984), Mineralogy and composition of the upper mantle, *Geophys. Res. Lett.*, *11*, 637–640, doi:10.1029/GL011i007p00637.

Anderson, D. L., and C. Sammis (1970), Partial melting in the upper mantle, *Phys. Earth Planet. Inter.*, *3*, 41–50, doi:10.1016/0031-9201(70)90042-7.

Ballmer, M. D., J. van Hunen, G. Ito, P. J. Tackley, and T. A. Bianco (2007), Non-hotspot volcano chains originating from small-scale sublithospheric convection, *Geophys. Res. Lett.*, *34*, L23310, doi:10.1029/2007GL031636.

Bonatti, E., and C. G. A. Harrison (1976), Hot lines in the Earths mantle, *Nature*, *263*, 402–404.

Bonatti, E., C. G. A. Harrison, D. E. Fisher, J. Honnorez, J. G. Schilling, J. J. Stipp, and M. Zentilli (1977), Easter volcanic chain (southeast Pacific): A mantle hot line, *J. Geophys. Res.*, *82*, 2457–2478.

Bonneville, A., R. Le Suave, L. Audin, V. Clouard, L. Dosso, P. Y. Gillot, P. Janney, K. Jordahl, and K. Maamaatuaiahutapu (2002), Arago Seamount: The missing hotspot found in the Austral Islands, *Geology*, *30*, 1023–1026.

Bonneville, A., L. Dosso, and A. Hildenbrand (2006), Temporal evolution and geochemical variability of the South Pacific superplume activity, *Earth Planet. Sci. Lett.*, *244*, 251–269.

Buck, W. R., and E. M. Parmentier (1986), Convection beneath young oceanic lithosphere: Implications for thermal structure and gravity, *J. Geophys. Res.*, *91*, 1961–1974, doi:10.1029/JB091iB02p01961.

Cadek, O., and L. Fleitout (2003), Effect of lateral viscosity variations in the top 300 km on the geoid and dynamic topography, *Geophys. J. Int.*, *152*, 566–580, doi:10.1046/j.1365-246X.2003.01859.x.

Chauvel, C., W. McDonough, G. Guille, R. Maury, and R. Duncan (1997), Contrasting old and young volcanism in Rurutu Island, Austral chain, *Chem. Geol.*, *139*, 125–143.

Christensen, U. (1984), Convection with pressure-dependent and temperature-dependent non-Newtonian rheology, *Geophys. J. R. Astron. Soc.*, *77*, 343–384.

Christensen, U. R., and D. A. Yuen (1985), Layered convection induced by phase transitions, *J. Geophys. Res.*, *90*, 10,291–10,300, doi:10.1029/JB090iB12p10291.

Clouard, V., and A. Bonneville (2005), Ages of seamounts, islands, and plateaus on the Pacific plate, in *Plumes, Plates, and Paradigms*, *Spec. Pap. Geol. Soc. Am.*, *388*, 71–90.

Clouard, V., and M. Gerbault (2008), Reply to "Break-up spots: Could the Pacific open as a consequence of plate kinematics?" comment by R. Pilger, *Earth Planet. Sci. Lett.*, *275*, 196–199, doi:10.1016/j.epsl.2008.08.008.

Conrad, C. P., and P. Molnar (1999), Convective instability of a boundary layer with temperature- and strain-rate-dependent viscosity in terms of "available buoyancy," *Geophys. J. Int.*, *139*, 51–68, doi:10.1046/j.1365-246X.1999.00896.x.

Dasgupta, R., M. M. Hirschmann, and N. D. Smith (2007), Partial melting experiments of peridotite CO_2 at 3 GPa and genesis of alkalic ocean island basalts, *J. Petrol.*, *48*, 2093–2124.

Davaille, A. (1999), Simultaneous generation of hotspots and superswells by convection in a heterogeneous planetary mantle, *Nature*, *402*, 756–760, doi:10.1038/45461.

Davaille, A., and C. Jaupart (1993), Transient high-Rayleigh-number thermal-convection with large viscosity variations, *J. Fluid Mech.*, *253*, 141–166, doi:10.1017/S0022112093001740.

Davis, A. S., L. B. Gray, D. A. Clague, and J. R. Hein (2002), The Line Islands revisited: New $^{40}Ar/^{39}Ar$ geochronologic evidence for episodes of volcanism due to lithospheric extension, *Geochem. Geophys. Geosyst.*, *3*(3), 1018, doi:10.1029/2001GC000190.

Dumoulin, C., M. P. Doin, and L. Fleitout (2001), Numerical simulations of the cooling of an oceanic lithosphere above a convective mantle, *Phys. Earth Planet. Inter.*, *125*, 45–64, doi:10.1016/S0031-9201(01)00233-3.

Dumoulin, C., M. P. Doin, D. Arcay, and L. Fleitout (2005), Onset of small-scale instabilities at the base of the lithosphere: Scaling laws and role of pre-existing lithospheric structures, *Geophys. J. Int.*, *160*, 345–357, doi:10.1111/j.1365-246X.2004.02475.x.

Dumoulin, C., G. Choblet, and M. P. Doin (2008), Convective interactions between oceanic lithosphere and asthenosphere: Influence of a transform fault, *Earth Planet. Sci. Lett.*, *274*, 301–309, doi:10.1016/j.epsl.2008.07.017.

Duncan, R. A., and I. McDougall (1976), Linear volcanism in French Polynesia, *J. Volcanol. Geotherm. Res.*, *1*, 197–227.

Faul, U. H. (2001), Melt retention and segregation beneath mid-ocean ridges, *Nature*, *410*, 920–923, doi:10.1038/35073556.

Faul, U. H., and I. Jackson (2005), The seismological signature of temperature and grain size variations in the upper mantle, *Earth Planet. Sci. Lett.*, *234*, 119–134, doi:10.1016/j.epsl.2005.02.008.

Foulger, G. R. (2007), The "Plate" model for the origin of melting anomalies, in *Plates, Plumes, and Planetary Processes*, edited by G. R. Foulger and D. M. Jurdy, *Spec. Pap. Geol. Soc. Am.*, *430*, 1–28.

Gans, K. D., D. S. Wilson, and K. C. Macdonald (2003), Pacific Plate gravity lineaments: Diffuse extension or thermal contraction?, *Geochem. Geophys. Geosyst.*, *4*(9), 1074, doi:10.1029/2002GC000465.

Goodwillie, A. M. (1995), Short-wavelength gravity lineations and unusual flexure results at the Puka Puka volcanic ridge system, *Earth Planet. Sci. Lett.*, *136*, 297–314.

Griffiths, R. W., and I. H. Campbell (1991), Interaction of mantle plume heads with the Earths surface and onset of small-scale convection, *J. Geophys. Res.*, *96*, 18,295–18,310, doi:10.1029/91JB01897.

Harmon, N., D. W. Forsyth, and D. S. Scheirer (2006), Analysis of gravity and topography in the GLIMPSE study region:

Isostatic compensation and uplift of the Sojourn and Hotu Matua Ridge systems *J. Geophys. Res.*, *111*, B11406, doi:10.1029/2005JB004071.

Harmon, N., D. W. Forsyth, R. Lamm, and S. C. Webb (2007), P and S wave delays beneath intraplate volcanic ridges and gravity lineations near the East Pacific Rise, *J. Geophys. Res.*, *112*, B03309, doi:10.1029/2006JB004392.

Haxby, W. F., and J. K. Weissel (1986), Evidence for small-scale mantle convection from Seasat altimeter data, *J. Geophys. Res.*, *91*, 3507–3520, doi:10.1029/JB091iB03p03507.

Hernlund, J. W., P. J. Tackley, and D. J. Stevenson (2008), Buoyant melting instabilities beneath extending lithosphere: 1. Numerical models, *J. Geophys. Res.*, *113*, B04405, doi:10.1029/2006JB004862.

Herzberg, C., P. D. Asimow, N. Arndt, Y. L. Niu, C. M. Lesher, J. G. Fitton, M. J. Cheadle, and A. D. Saunders (2007), Temperatures in ambient mantle and plumes: Constraints from basalts, picrites, and komatiites, *Geochem. Geophys. Geosyst.*, *8*, Q02006, doi:10.1029/2006GC001390.

Hillier, J. K., and A. B. Watts (2004), "Plate-like" subsidence of the East Pacific Rise–South Pacific superswell system, *J. Geophys. Res.*, *109*, B10102, doi:10.1029/2004JB003041.

Hirth, G., and D. L. Kohlstedt (1996), Water in the oceanic upper-mantle: Implications for rheology, melt extraction and the evolution of the lithosphere, *Earth Planet. Sci. Lett.*, *144*, 93–108, doi:10.1016/0012-821X(96)00154-9.

Hirth, G., and D. L. Kohlstedt (2003), Rheology of the upper mantle and mantle wedge: A view from the experimentalists, in *Inside the Subduction Factory*, *Geophys. Monogr. Ser.*, vol. 138, edited by J. Eiler, pp. 83–105, AGU, Washington, D. C.

Huang, J., and S. Zhong (2005), Sublithospheric small-scale convection and its implications for the residual topography at old ocean basins and the plate model, *J. Geophys. Res.*, *110*, B05404, doi:10.1029/2004JB003153.

Huang, J. S., S. J. Zhong, and J. van Hunen (2003), Controls on sublithospheric small-scale convection, *J. Geophys. Res.*, *108*(B8), 2405, doi:10.1029/2003JB002456.

Ito, G., and J. J. Mahoney (2005), Flow and melting of a heterogeneous mantle: 1. Method and importance to the geochemistry of ocean island and mid-ocean ridge basalts, *Earth Planet. Sci. Lett.*, *230*, 29–46, doi:10.1016/j.epsl.2004.10.035.

Janney, P. E., and P. R. Castillo (1999), Isotope geochemistry of the Darwin Rise seamounts and the nature of long-term mantle dynamics beneath the south central Pacific, *J. Geophys. Res.*, *104*, 10,571–10,589.

Janney, P. E., J. D. Macdougall, J. H. Natland, and M. A. Lynch (2000), Geochemical evidence from the Pukapuka volcanic ridge system for a shallow enriched mantle domain beneath the South Pacific Superswell, *Earth Planet. Sci. Lett.*, *181*, 47–60, doi:10.1016/S0012-821X(00)00181-3.

Karato, S. (1986), Does partial melting reduce the creep strength of the upper mantle?, *Nature*, *319*, 309–310, doi:10.1038/319309a0.

Karato, S., and H. Jung (1998), Water, partial melting and the origin of the seismic low velocity and high attenuation zone in the upper mantle, *Earth Planet. Sci. Lett.*, *157*, 193–207, doi:10.1016/S0012-821X(98)00034-X.

Karato, S. I., M. S. Paterson, and J. D. Fitzgerald (1986), Rheology of synthetic olivine aggregates - Influence of grain-size and water, *J. Geophys. Res.*, *91*, 8151–8176, doi:10.1029/JB091iB08p08151.

Katz, R. F., M. Spiegelman, and C. H. Langmuir (2003), A new parameterization of hydrous mantle melting, *Geochem. Geophys. Geosyst.*, *4*(9), 1073, doi:10.1029/2002GC000433.

Katz, R. F., M. Spiegelman, and B. Holtzman (2006), The dynamics of melt and shear localization in partially molten aggregates, *Nature*, *442*, 676–679.

Konter, J. G., B. B. Hanan, J. Blichert-Toft, A. A. P. Koppers, T. Plank, and H. Staudigel (2008), One hundred million years of mantle geochemical history suggest the retiring of mantle plumes is premature, *Earth Planet. Sci. Lett.*, *275*, 285–295, doi:10.1016/j.epsl.2008.08.023.

Koppers, A. A. P., H. Staudigel, M. S. Pringle, and J. R. Wijbrans (2003), Short-lived and discontinuous intraplate volcanism in the South Pacific: Hot spots or extensional volcanism?, *Geochem. Geophys. Geosyst.*, *4*(10), 1089, doi:10.1029/2003GC000533.

Koppers, A. A. P., H. Staudigel, J. Phipps Morgan, and R. A. Duncan (2007), Nonlinear $^{40}Ar/^{39}Ar$ age systematics along the Gilbert Ridge and Tokelau Seamount Trail and the timing of the Hawaii-Emperor Bend, *Geochem. Geophys. Geosyst.*, *8*, Q06L13, doi:10.1029/2006GC001489.

Korenaga, J., and T. H. Jordan (2003), Linear stability analysis of Richter rolls, *Geophys. Res. Lett.*, *30*(22), 2157, doi:10.1029/2003GL018337.

Korenaga, J., and T. H. Jordan (2004), Physics of multiscale convection in Earth's mantle: Evolution of sublithospheric convection, *J. Geophys. Res.*, *109*, B01405, doi:10.1029/2003JB002464.

Lee, C. T. A., A. Lenardic, C. M. Cooper, F. L. Niu, and A. Levander (2005), The role of chemical boundary layers in regulating the thickness of continental and oceanic thermal boundary layers, *Earth Planet. Sci. Lett.*, *230*, 379–395.

Lynch, M. A. (1999), Linear ridge groups: Evidence for tensional cracking in the Pacific Plate, *J. Geophys. Res.*, *104*, 29,321–29,334, doi:10.1029/1999JB900241.

Marquart, G. (2001), On the geometry of mantle flow beneath drifting lithospheric plates, *Geophys. J. Int.*, *144*, 356–372, doi:10.1046/j.0956-540X.2000.01325.x.

Marquart, G., H. Schmeling, and A. Braun (1999), Small-scale instabilities below the cooling oceanic lithosphere, *Geophys. J. Int.*, *138*, 655–666, doi:10.1046/j.1365-246x.1999.00885.x.

McKenzie, D. (1985), ^{230}Th-^{238}U disequilibrium and the melting processes beneath ridge axes, *Earth Planet. Sci. Lett.*, *72*, 149–157, doi:10.1016/0012-821X(85)90001-9.

McNutt, M. K. (1998), Superswells, *Rev. Geophys.*, *36*, 211–244.

McNutt, M. K., D. W. Caress, J. Reynolds, K. A. Jordahl, and R. A. Duncan (1997), Failure of plume theory to explain midplate volcanism in the southern Austral islands, *Nature*, *389*, 479–482.

Moresi, L., and M. Gurnis (1996), Constraints on the lateral strength of slabs from 3-dimensional dynamic flow models, *Earth Planet. Sci. Lett.*, *138*, 15–28, doi:10.1016/0012-821X(95)00221-W.

Morgan, W. J. (1971), Convection plumes in the lower mantle, *Nature*, *230*, 42–43, doi:10.1038/230042a0.

Morgan, W. J. (1972), Plate motions and deep mantle convection, *Mem. Geol. Soc. Am.*, *132*, 7–22.

Niu, Y. L., and M. J. O'Hara (2003), Origin of ocean island basalts: A new perspective from petrology, geochemistry, and mineral physics considerations, *J. Geophys. Res.*, *108*(B4), 2209, doi:10.1029/2002JB002048.

Oliver, D. S., and J. R. Booker (1983), Planform of convection with strongly temperature-dependent viscosity, *Geophys. Astrophys. Fluid Dyn.*, *27*, 73–85.

Parsons, B., and D. McKenzie (1978), Mantle convection and thermal structure of plates, *J. Geophys. Res.*, *83*, 4485–4496, doi:10.1029/JB083iB09p04485.

Phipps Morgan, J., and J. Morgan (1999), Two-stage melting and the geochemical evolution of the mantle: A recipe for mantle plum-pudding, *Earth Planet. Sci. Lett.*, *170*, 215–239, doi:10.1016/S0012-821X(99)00114-4.

Pilet, S., M. B. Baker, and E. M. Stolper (2008), Metasomatized lithosphere and the origin of alkaline lavas, *Science*, *320*, 916–919.

Priestley, K., and D. McKenzie (2006), The thermal structure of the lithosphere from shear wave velocities, *Earth Planet. Sci. Lett.*, *244*, 285–301.

Raddick, M. J., E. M. Parmentier, and D. S. Scheirer (2002), Buoyant decompression melting: A possible mechanism for intraplate volcanism, *J. Geophys. Res.*, *107*(B10), 2228, doi:10.1029/2001JB000617.

Richter, F. M. (1973), Convection and the large-scale circulation of the mantle, *J. Geophys. Res.*, *78*, 8735–8745, doi:10.1029/JB078i035p08735.

Richter, F. M., and B. Parsons (1975), On the interaction of two scales of convection in the mantle, *J. Geophys. Res.*, *80*(17), 2529–2541.

Sandwell, D., and Y. Fialko (2004), Warping and cracking of the Pacific plate by thermal contraction, *J. Geophys. Res.*, *109*, B10411, doi:10.1029/2004JB003091.

Sandwell, D. T., E. L. Winterer, J. Mammerickx, R. A. R. A. Duncan, M. A. Lynch, D. A. Levitt, and C. L. Johnson (1995), Evidence for diffuse extension of the Pacific plate from Pukapuka ridges and cross-grain gravity lineations, *J. Geophys. Res.*, *100*, 15,087–15,100, doi:10.1029/95JB00156.

Schellart, W. P., D. R. Stegman, and J. Freeman (2008), Global trench migration velocities and slab migration induced upper mantle volume fluxes: Constraints to find an Earth reference frame based on minimizing viscous dissipation, *Earth Sci. Rev.*, *88*, 118–144.

Schmeling, H. (2000), Partial melting and melt segregation in a convecting mantle, in *Physics and Chemistry of Partially Molten Rocks*, edited by N. Bagdassarov et al., pp. 141–178, Kluwer, Dortrecht, Netherlands.

Schmeling, H. (2006), A model of episodic melt extraction for plumes, *J. Geophys. Res.*, *111*, B03202, doi:10.1029/2004JB003423.

Schubert, G., G. Masters, P. Olson, and P. Tackley (2004), Superplumes or plume clusters?, *Phys. Earth Planet. Inter.*, *146*, 147–162.

Schutt, D. L., and C. E. Lesher (2006), Effects of melt depletion on the density and seismic velocity of garnet and spinel lherzolite, *J. Geophys. Res.*, *111*, B05401, doi:10.1029/2003JB002950.

Sleep, N. H. (2008), Channeling at the base of the lithosphere during the lateral flow of plume material beneath flow line hot spots, *Geochem. Geophys. Geosyst.*, *9*, Q08005, doi:10.1029/2008GC002090.

Smith, W. H. F., H. Staudigel, A. B. Watts, and M. S. Pringle (1989), The Magellan seamounts: Early Cretaceous record of the South Pacific Isotopic and Thermal Anomaly, *J. Geophys. Res.*, *94*, 10,501–10,523, doi:10.1029/JB094iB08p10501.

Sobolev, A. V., et al. (2007), The amount of recycled crust in sources of mantle-derived melts, *Science*, *316*, 412–417.

Staudigel, H., K. H. Park, M. Pringle, J. L. Rubenstone, W. H. F. Smith, and A. Zindler (1991), The longevity of the South Pacific isotopic and thermal anomaly, *Earth Planet. Sci. Lett.*, *102*, 24–44, doi:10.1016/0012-821X(91)90015-A.

Stevenson, D. J. (1989), Spontaneous small-scale melt segregation in partial melts undergoing deformation, *Geophys. Res. Lett.*, *16*, 1067–1070, doi:10.1029/GL016i009p01067.

Stixrude, L., and C. Lithgow-Bertelloni (2005), Mineralogy and elasticity of the oceanic upper mantle: Origin of the low-velocity zone, *J. Geophys. Res.*, *110*, B03204, doi:10.1029/2004JB002965.

Stracke, A., B. Bourdon, and D. McKenzie (2006), Melt extraction in the Earth's mantle: Constraints from U-Th-Pa-Ra studies in oceanic basalts, *Earth Planet. Sci. Lett.*, *244*, 97–112.

Tackley, P. J., and D. J. Stevenson (1993), A mechanism for spontaneous self-perpetuating volcanism on the terrestrial planets, in *Flow and Creep in the Solar System: Observations, Modeling and Theory*, edited by D. B. Stone and S. K. Runcorn, pp. 307–322, Kluwer, Dordrecht, Netherlands.

Turner, D. L., and R. D. Jarrard (1982), K-Ar dating of the Cook-Austral chain—A test of the hot-spot hypothesis, *J. Volcanol. Geotherm. Res.*, *12*, 187–220.

van Hunen, J., and S. Zhong (2006), Influence of rheology on realignment of mantle convective structure with plate motion after a plate reorganization, *Geochem. Geophys. Geosyst.*, *7*, Q08008, doi:10.1029/2005GC001209.

van Hunen, J., J. S. Huang, and S. J. Zhong (2003), The effect of shearing on the onset and vigor of small-scale convection in a Newtonian rheology, *Geophys. Res. Lett.*, *30*(19), 1991, doi:10.1029/2003GL018101.

van Hunen, J., S. J. Zhong, N. M. Shapiro, and M. H. Ritzwoller (2005), New evidence for dislocation creep from 3-D geodynamic modeling of the Pacific upper mantle structure, *Earth Planet. Sci. Lett.*, *238*, 146–155.

van Keken, P. E. (1993), Numerical Modeling of Thermochemically Driven Flow With Non-Newtonian Rheology: Applied to the Earth's Lithosphere and Mantle, *Geol. Ultraiectina*, *107*, 26–27.

Weeraratne, D. S., D. W. Forsyth, Y. Yang, and S. C. Webb (2007), Rayleigh wave tomography beneath intraplate volcanic ridges in the South Pacific, *J. Geophys. Res.*, *112*, B06303, doi:10.1029/2006JB004403.

Zaranek, S. E., and E. M. Parmentier (2004), Convective cooling of an initially stably stratified fluid with temperature-dependent viscosity: Implications for the role of solid state convection in planetary evolution, *J. Geophys. Res.*, *109*, B03409, doi:10.1029/2003JB002462.

Zhong, S., M. T. Zuber, L. Moresi, and M. Gurnis (2000), Role of temperature-dependent viscosity and surface plates in spherical shell models of mantle convection, *J. Geophys. Res.*, *105*, 11,063–11,082, doi:10.1029/2000JB900003.

Zou, H. B. (1998), Trace element fractionation during modal and nonmodal dynamic melting and open-system melting: A mathematical treatment, *Geochim. Cosmochim. Acta*, *62*, 1937–1945.